

FABRICATION OF CMUTS BASED ON PMMA ADHESIVE WAFER BONDING

by

Mansoor Ahmad

Submitted to the Graduate School of Engineering and Natural Sciences
in partial fulfillment of
the requirements for the degree of
Doctor of Philosophy

Sabanci University

July, 2019

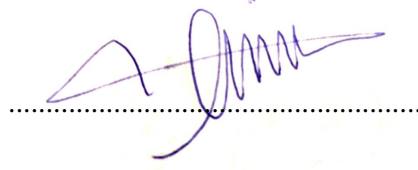
FABRICATION OF CMUTS BASED ON PMMA ADHESIVE WAFER
BONDING

APPROVED BY:

Assoc. Prof. Dr. Ayhan BOZKURT
(Thesis Supervisor)



Prof. Dr. İbrahim TEKİN



Assoc. Prof. Dr. Ahmet ONAT



Assoc. Prof. Dr. Gökseın Gökseınin YARALIOĞLU
(Özyeğın Üniversitesi)



Assoc. Prof. Dr. Arif Sanlı ERGÜN
(TOBB ETÜ)



DATE OF APPROVAL: 19.07.2019

© Mansoor Ahmad 2019
All Rights Reserved

To my Grandparents, Parents, Parents-in-law, and Family

Acknowledgments

Praise be to ALLAH, the Cherisher and the Sustainer of the worlds. (The Holy Quran 1:1)

I am grateful to my dissertation advisor Assoc. Prof. Dr. Ayhan Bozkurt for his help, support and patience. The accomplishments in this dissertation would not have been possible without his guidance and encouragements. I would like to express my sincere gratitude to him for not only his continuous guidance during these years but also for providing a perfect example of an academician, an advisor, and a humble human being.

I am thankful to the members of my dissertation committee, Prof. Dr. İbrahim Tekin, Assoc. Prof. Dr. Ahmet Onat, Assoc. Prof. Dr. Göksen Göksenin Yaralıoğlu, and Assoc. Prof. Dr. Arif Sanlı Ergün, for careful evaluation of my work and providing useful comments to improve the quality of this dissertation. I was very fortunate to have Dr. Omid Farhanieh as a continuous resource, his in-depth experimental characterization skills have greatly influenced this dissertation. I am grateful to Dr. Rupak Roy, his clean room experience with micro-machining have been instrumental to tackle many problems. I am also grateful to the Higher Education Commission of Pakistan (HEC Pakistan) for supporting me under the HRDI- FACULTY DEVELOPMENT of UESTPS-UETS program. I am very grateful and thankful to Abdul Munem Khattak for his support and being my guarantor to secured the HEC scholarship offer.

I am also thankful to Ammar Saleem, Akhtar Saeed, Muhammad Omer Asim, and Milad Diba for their interaction and insightful discussions which greatly contributed to this work. I am thankful to Rayan Bajwa for thoughtful discussions and sharing experience of the clean room. I am also grateful to SUNUM and FENS-EE lab specialists, Onur Serbest, Ali Kasal and Sercan Tanyeli for their continuous support.

I am profoundly indebted to many of my great friends including Muhammad Ayat, Muhammad Yaqoob Khan, Raja Muhammad Awais, Muhammad Sohaib Amjad, Fiaz Ahmad, Muhammad Usman Ghani, and Waqar Ahmed for their countless favors. I am thankful to Ayat for the care, guidance and encouragement, I thank him for his company to travel through some of the beautiful places of the country, it is because of him that I have explored some of the other cities of Turkey. I am grateful to Sohaib, Fiaz and Usman for the two great years of support and guidance we spent together. I am thankful to Fiaz Ahmad and Hafiz Qasim Ali for being my roommates. I am grateful to all of them for their confidence in my work.

I would like to deeply thank my family for all their loves and supports. My parents have supported me so much, so I could be where I am today. Nothing would have ever been possible without their endless support and love. Thanks to my sisters and my brother Sadiq for their supports. I am grateful to my uncles, aunts and cousins specially Asad for their emotional support, kindness and encouragements. I would also like to express my gratitude to my parents-in-law for all their supports and understandings. Finally and most importantly, I would like to express my deepest gratitude to my wife and my daughter, Javeera Ahmad, whose unlimited encouragement and patience has been the greatest source of energy for me to keep going forward during the entire journey of my Ph.D.

I want to recognize many individuals whose names I could not mention here, who have profoundly affected me and helped me shape my thoughts and believes.

FABRICATION OF CMUTS BASED ON PMMA ADHESIVE WAFER BONDING

Mansoor Ahmad

EE, Ph.D. Dissertation, 2019

Thesis Supervisor: Assoc. Prof. Dr. Ayhan BOZKURT

Keywords: Capacitive Micromachined Ultrasonic Transducers (CMUTs); wafer bonding; PMMA; Microelectromechanical Systems (MEMS)

Abstract

Capacitive Micromachined Ultrasonic Transducers (CMUTs) are the potential alternatives for the conventional piezoelectric ultrasonic transducers. CMUTs have been under an extensive research and development since their first development in the mid-1990s. Initially developed for air-coupled applications, CMUTs have shown far better acceptability in immersion-based applications (i.e. medical ultrasonic imaging, medical therapy, and underwater imaging) when compared to the piezoelectric ultrasonic transducers.

CMUTs are parallel-plate capacitors fabricated using the Micro Electro Mechanical Systems (MEMS) technology. Despite of the fact that various CMUT fabrication methods have been reported in the literature, there are still many challenges to address in CMUTs design and fabrication. Standard fabrication techniques are further sub-divided into the Sacrificial Layer Release Process and the Wafer Bonding methods. A number of complications are associated with these techniques, such as optimization of the design parameters, process complexity, sacrificial layer material with the corresponding etchant selection, wafer cost and selection. In particular, the sacrificial release methods consist of complex fabrication steps. Furthermore, structural parameters like gap height and radius have optimization issues during the sacrificial release process. On the other hand, the wafer bonding techniques for the CMUTs fabrication are simple and have a great control over the structure parameters in contrast to the sacrificial release methods. At the same time, the wafer-bonded CMUTs require very high quality wafer

surface and have a very high contamination sensitivity. For this purpose, this dissertation aims to develop a simple, low cost and lower constraint thermocompression-based technique for the CMUT fabrication.

The proposed wafer bonding technique for the CMUT fabrication in the dissertation uses Polymethyl methacrylate (PMMA) adhesive as an intermediate layer for the thermocompression wafer bonding. The advantages associated with the PMMA adhesive-based wafer bonding over the other wafer bonding methods include low process temperature (usually 200 °C or less), high wafer surface defects and contamination tolerance, high surface energy and low bonding stresses. These factors will add cost effectiveness and simplicity to the CMUTs fabrication process. Furthermore, the achieved receive sensitivity with the reported CMUT is found comparable to the commercially available ultrasonic transducers.

PMMA YAPIŞTIRICILI PUL BAĞLAMA YÖNTEMİYLE KAPASİTİF MİKROİŞLENMİŞ ULTRASONİK GÜÇ ÇEVİRİCİ (CMUT) ÜRETİMİ

Mansoor Ahmad

EE, Doktora Tezi, 2019

Tez Danışmanı: Doç. Dr. Ayhan BOZKURT

Anahtar Kelimeler: Kapasitif Mikroişlenmiş Ultrasonik Güç Çeviriciler (CMUTlar); pul bağlama; PMMA, mikroeletromekanik sistemler (MEMS)

Özet

Kapasitif Mikroişlenmiş Ultrasonik Güç Çeviriciler (CMUTlar) geleneksel piezoelektrik ultrason dönüştürücülerine bir alternatif teşkil etmektedir. CMUTlar, ilk öncelendikleri 1990'ların ortalarında beri kapsamlı olarak araştırılıp geliştirilmektedir. İlk başta hava ortamında kullanılmak için geliştirilmiş olsalar da, sıvıya daldırılmış şekildeki uygulamalarda (tıbbi ultrason görüntüleme, tıbbi sağaltım ve sualtı görüntüleme gibi) çok daha fazla kabul görür olmuşlardır.

CMUTlar mikroeletromekanik sistem (MEMS) teknolojisi kullanılarak üretilen paralel levha kondansatörleridir. Literatürde çeşitli CMUT üretim teknikleri mevcut olsa da, bu cihazların üretiminde hâlâ aşılması gereken birçok sorun bulunmaktadır. Standart üretim teknikleri kurban tabaka bırakımı ve pul bağlama olarak iki alt kategoriye ayrılmaktadır. Bu üretim teknikleriyle ilgili zorluklar; tasarım parametrelerinin en iyi hale getirilmesi, işlem karmaşıklığı, kurban tabaka ve karşılık gelen aşındırıcı seçimi, pul masrafı ve seçimi olarak sıralanabilir. Özellikle kurban tabaka bırakımı yöntemleri karmaşık üretim aşamaları barındırmaktadır. Ayrıca boşluk yüksekliği ve yarıçapı gibi yapısal parametrelerin optimizasyonunda kurban tabaka bırakımı sırasında sorunlar yaşanmaktadır. Öte yandan, pul bağlama teknikleri kurban tabaka bırakımı yöntemlerine kıyasla basitlikleri ve yapı parametreleri üzerinde daha fazla kontrol sahibi olma bakımından daha avantajlıdır. Ama pul bağlama teknikleri ile üretilen CMUTlar için yüksek kaliteli pul yüzeyi gerekmektedir ve bu teknikler pul yüzeyinin temizliğine çok hassastır. Bu sebeplerden dolayı, bu tezde basit, ucuz ve daha az kısıtlı bir ısıl sıkıştırma tabanlı CMUT üretim tekniği geliştirilmesi amaçlanmıştır.

CMUT üretimi için önerilen pul bağlama tekniğinde polimetil metakrilat (PMMA) yapıştırıcısı ısı sıkıştırılmalı pul bağlama sürecinde bir ara tabaka olarak kullanılmaktadır. PMMA-bazlı pul bağlama tekniğinin diğer tekniklere göre avantajları düşük işlem sıcaklığı (genelde 200 °C ya da daha düşük sıcaklık), puldaki kusur ve yüzey kirliliğine yüksek tolerans, yüksek yüzey enerjisi ve düşük bağlama stresidir. Bu faktörler CMUT üretiminin verimliliğine ve basitliğine katkı sağlamaktadır. Üretilen CMUTların alışı hassasiyeti, ticari olarak mevcut ultrasonik dönüştürücülerle karşılaştırılabilir seviyede bulunmuştur.

Table of Contents

Acknowledgments	v
Abstract	vii
Özet	ix
1 Introduction	1
1.1 Problem Definition and Motivation	1
1.2 Contributions of this Thesis	4
1.3 Organization of the Dissertation	5
2 Background	6
2.1 CMUTs Fabrication Technologies	7
2.1.1 Sacrificial Layer Release Process	7
2.1.2 Wafer Bonding	8
2.2 Selection of CMUT Fabrication Method	14
2.2.1 Selection of Polymer adhesive for CMUT Fabrication	14
2.2.2 Advantages and Disadvantages of Polymer Bonding	15
3 Design and Fabrication	16
3.1 Design of CMUTs	16
3.1.1 Design Methodology	16
3.1.2 Analytical Modeling	17
3.2 Fabrication of CMUTs	20
3.2.1 Mask Preparation	21
3.2.2 Micro-Machining Steps	22
3.2.3 Wafers Thermocompression Bonding	24
3.3 Thermocompression Bonder	26
3.3.1 Wafer Bonding Process	29
3.4 Preliminary Testing and Packaging	31
3.5 Bonding Quality	32
3.6 Comparison of the Developed Fabrication Technique to the Existing Fabrication Techniques	32

4	Characterization	34
4.1	Static Characterization	34
4.1.1	Impedance Analyzer Analysis	34
4.1.2	Optical Profilometer Analysis	36
4.2	Dynamic Acoustic Characterization	38
4.2.1	Bandwidth	39
4.2.2	Sensitivity	39
5	Conclusion and Future Work	43
5.1	Conclusion	43
5.2	Discussion and Future Work	44
5.2.1	Patterning Cavities in the Adhesive PMMA Layer	44
5.2.2	Membrane Silicon Layer Etching	45
5.2.3	Explore new Adhesive Materials	45
A	Finite Element Analysis	46
B	Squeeze Film Damping	48
	Bibliography	51

List of Figures

1.1	Basic Working Principle of the CMUT	2
2.1	Process steps of the sacrificial release fabrication technique. (a) Image reversal lithography with sacrificial mask on insulating nitride; (b) DRIE defines the sacrificial cavity; (c) Chromium deposition into the sacrificial layer; (d) Liftoff and cleaning; (e) Membrane deposition; (f) Top electrode deposition; (g) Burying electrode under thick nitride; (h) Etch holes patterning; (i) Sacrificial under-etch and release; (j) Final cavity sealing. Reprinted from [48].	8
2.2	Process flow for direct wafer bonding CMUT. (a) Prime wafer; (b) Oxidation; (c) Cavity formation; (d) Thermal oxidation; (e) SOI wafer bonding; (f) SOI handle; (g) Removing BOX; (h) Metallization; (i) Electrode pattern and device isolation. Reprinted from [52].	10
2.3	Metal-bonded CMUT process flow. (a) Oxidation; (b) Etching to form insulation layer; (c) Central insulation block; (d) Metal layer; (e) Metal layer on silicon wafer; (f) Wafer bonding; (g) Etching the handle silicon; (h) Etching the BOX; (i) Aluminum deposition and etching for metal pads. © 2015 IEEE [54].	12
2.4	Anodic bonding process flow. (a-d) Thermal oxidation and oxide etching for cavity formation; (e-h) Etching glass, bottom electrode formation, and cleaning; (i) Anodic bonding. © 2012 IEEE [57].	13
3.1	Effect on membrane deflection against membrane radial position for different ambient pressure levels.	19

3.2	Top (left) and cross-sectional (right) views of the proposed Capacity Micromachined Ultrasonic Transducer (CMUT), showing device dimensions. Reprinted from [73].	20
3.3	Photo mask. (a) The acetate mask used in lithography process to produce the final mask; (b) The final quartz mask.	22
3.4	Surface Micro-machining steps for CMUT fabrication. (a) Thermally grown oxide wafer; (b) Spun coated photoresist; (c) CMUTs shape development using photolithography; (d) DRIE etched oxide layer for cavity formation; (e) PMMA spun coated second oxide wafer.	24
3.5	Process steps for CMUT fabrication. (a) Pattern lithography and developing; (b) Oxide etching and cleaning; (c) Polymethyl methacrylate (PMMA) coating; (d) Membrane and cavity alignment and bonding; (e) Final structure. Reprinted from [73].	25
3.6	The developed thermocompression bonder. Schematic (left). Actual (right)	26
3.7	Embodiments inside the chamber. (A) Compression screw; (B) Support springs; (C) Supporting ceramic plate; (D) Aluminium fixture for bonding elements; (E) Bonding elements (Thermal and compression).	27
3.8	Bonder elements. (A) Compression contact; (B) Compression element. (1) Aluminium slab; (2) Thermally insulating ceramic slab; (3) Compression contact ball; (4) Ceramic to aluminium adhesion composite; (C) Thermal elements. (1) Upper Aluminium block; (2) Lower Aluminium block; (3) The heating elements (5 are inserted into the upper Aluminium block and 5 into the lower); (4) Holes with the heater are sealed with white cement; (5) Bond interface; (6) Thermally insulating ceramic slab between thermal element and Aluminium fixture.	28
3.9	Side-view displaying the (A) (1) Thermocouple; and (B)-(C) Epoxy sealed duct for wire passage.	29
3.10	Manufactured cantilever for compression force calibration.	30
3.11	Device during fabrication stages. (a) Before bonding; (b) Final device; (c) Schematic of the final device. Reprinted from [73].	31

4.1	Impedance analyzer measurements	35
4.2	Pre-bonding optical profilometer measurements	36
4.3	Post-bonding and un-bonding optical profilometer measurements	37
4.4	Setup for pitch-catch experiment. Reprinted from [73]	38
4.5	Output signal of RX-CMUT for a tone burst of 15 cycles at 200 kHz (left), normalized magnitude for a frequency sweep from 100 to 300 kHz (right). Reprinted from [73].	39
4.6	Comparison of experimental and analytical unamplified output signal (left), corresponding acoustic pressure (right). Reprinted from [73].	41
4.7	Simulated RX-CMUT output with varying bias voltage (left); associated sensitivity (right). Reprinted from [73].	42
A.1	Side view (with reduced element count) and top view of FEA model. Reprinted from [73].	46

List of Tables

3.1	CMUT design Parameters	21
3.2	Silicon Dioxide Etching Parameters	25
3.3	Comparison of fabrication methods.	33
4.1	DC Bias Vs Output Sensitivity Comparison	42
A.1	Simulation parameters.	47
B.1	Squeeze-number computation parameters.	49
B.2	Squeeze number at different pressure levels.	49

Chapter 1

Introduction

This dissertation presents a new wafer bonded CMUT fabrication method based on PMMA adhesive thermocompression bonding. This chapter starts with an introduction to the CMUT, followed by various applications and fabrication techniques. Then, the motivation behind this research is described, and an overview of the contributions of this dissertation is discussed. Finally, the structure of this dissertation is provided.

1.1 Problem Definition and Motivation

Capacitive Micro-machined Ultrasonic Transducers (CMUTs) was introduced in 1994, as an alternate to the conventional piezoelectric-based transducers [1, 2]. Basically, CMUTs are two parallel-plate capacitors used for ultrasonic transduction. The basic structured single cell of CMUT is composed of a conducting bottom layer and a membrane top layer suspended over a sealed vacuum cavity. The bottom layer is a fixed silicon substrate while the top layer is a flexible plate. The two layers are isolated by a middle insulation layer and a shallow sealed cavity is formed within the insulation layer. The membrane have the ability to vibrate and hence forming a variable capacitor. As a transmitter, the membrane vibrates to produce ultrasonic signal when subject to alternating voltage pulses. In receiving mode, the membrane vibrates as a result of the incoming ultrasonic waves, which changes the capacitance of the transducer and, in turn, produces an electric signal. A typical CMUT and its working principle is

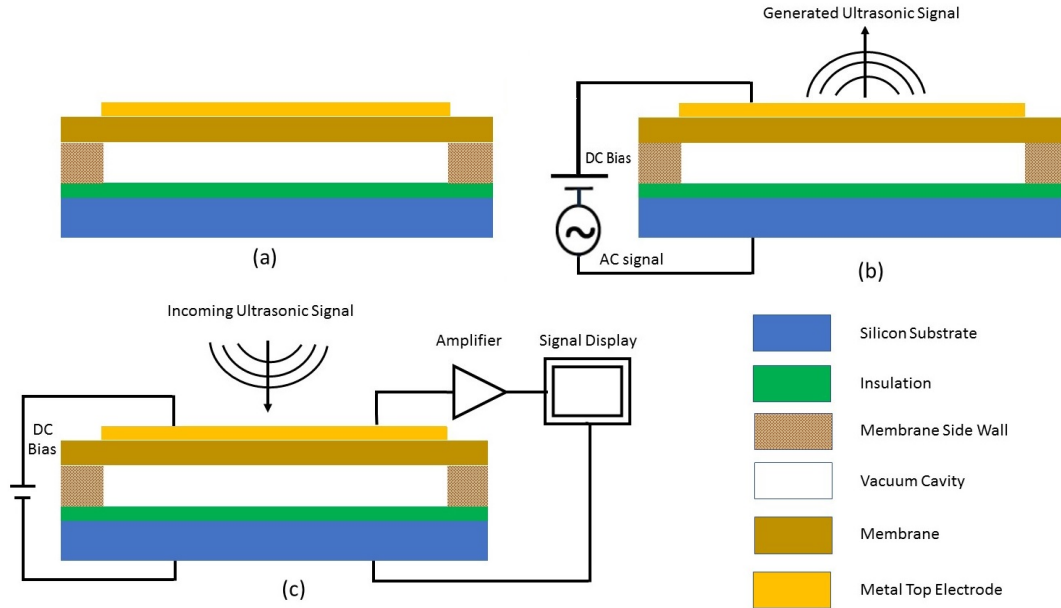


Figure 1.1: Basic Working Principle of the CMUT

described in Figure 1.1.

Initially produced for air-coupled ultrasonic applications, CMUTs, late on, have been adopted for immersion applications, such as medical ultrasonic imaging and underwater imaging [3, 4, 5, 6]. CMUTs offer better axial resolution due to its broader fractional bandwidth when compared to piezoelectric devices [7, 8]. Furthermore, unlike piezoelectric devices, the use of micro-fabrication technology makes the CMUTs fabrication process very simple and precise transducers can be fabricated in array form [9]. Also, adopting a low temperature fabrication technique makes it possible for the CMUTs to be integrated with Complementary Metal–Oxide–Semiconductor (CMOS) technology [10, 11, 12]. CMOS compatibility is highly desirable as the circuitry integrated with CMUTs would reduce the parasitics and, hence, enhance the performance of the CMUT [13, 14, 15, 16]. Thus, CMUTs have captured a lot of interest as an alternative to piezoelectric devices and have been under development since its first introduction. In addition to imaging, CMUTs have also been studied for other applications such as fluid density measurement [17], fluid sensing [18, 19], catheter ablation [20], tumor treatment [21], therapy [22, 23], flow measurement [24, 25] and distance sensing [26].

Besides all the advantages, a number of complications and limitations have been associated with the CMUT technology. For instance, compared to the piezoelectric devices, CMUTs have low output power in transmit mode. Furthermore, CMUTs have issues like acoustic cross-talk, and durability and reliability due to dielectric charging which need to be addressed [27, 28]. Researchers have showed huge interest in the development and optimization of the CMUTs to minimize the associated limitations [29, 30, 31, 32, 33, 34]. All of the design optimization studies need fabrication of CMUTs for experimental analysis and validation.

The first method adopted for fabrication of CMUTs was the sacrificial release process. In this process, the cavity is created by etching the sacrificial layer between the substrate and membrane layers [2]. There are some problems associated with the sacrificial release process, such as, the uniformity of the cavity during the under-etching process and the lack of control over the membrane thickness. Moreover, the suspending membrane may stick to the substrate during the sacrificial release process, specially for applications where a relatively thin membrane or an extremely small gap height is required. To overcome these problems, direct wafer bonding based CMUTs fabrication technique was demonstrated by Huang et al. [35]. The direct wafer bonding technique provided better uniformity and control at the cost of using the expensive Silicon-on-Insulator, (SOI), wafers. There are some drawbacks associated with the direct wafer bonding process, for example, the process has a very high sensitivity to surface roughness and contamination. Also, temperatures in excess of 1000 °C are required to carry out the bonding process. The high temperature problem was addressed by introducing the anodic wafer bonding technique [36]. Anodic bonding requires a high voltage (around 500 V) during the bonding process which makes the bonding system complicated. In short, the CMUTs fabrication techniques reported in the literature have several limitations such as the process complexity, wafer cost, surface roughness, and process control. In recent years, researchers have been developing the adhesives based wafers bonding techniques for CMUTs fabrication [37, 38, 39, 40]. The adhesive, which is spin coated on the surface of the wafer in fluid form, covers minor contamination and surface roughness, and hence, obviates expensive SOI wafers and complex surface

treatment steps. Henceforth, the prime motivation of the dissertation is to develop a low cost CMUT fabrication process having less fabrication constraints, from both the material and the equipment standpoints. Moreover, the proposed CMUT fabrication process would also provide a guideline for the other researchers working in the field of acoustics engineering, to further modify and optimize the proposed CMUT design as per the application needs.

1.2 Contributions of this Thesis

The major contribution of this dissertation is the process development and demonstration of CMUT fabrication using PMMA adhesive based thermocompression wafer bonding. Thermally grown silicon-oxide wafers have been successfully bonded to another silicon-oxide wafer using a lab-built thermocompression bonder. The presented CMUT is an unconventional wafer bonded device where the entire thickness of the silicon wafer has been used as a membrane and was developed to be used for underwater applications. The characterizations were performed in immersion for output power, receive sensitivity, resonance frequency and bandwidth calculations. The receive sensitivity of the developed CMUT is comparable to commercially available hydrophones [41]. Additionally, the proposed method minimizes the steps involved in the fabrication of the CMUT. Hence, the reported method is among the simplest ones as compared with the other formerly-reported methods, which results in much less fabrication time as well as the lower cost. Furthermore, fabrication methods to achieve high frequency and CMOS integrable CMUTs with PMMA adhesive based wafer bonding have also been suggested. As a consequence, researchers as well as the prospective students working in our laboratory could be guided on prospective works of polymers based wafer-bonded CMUTs development and the allied applications.

1.3 Organization of the Dissertation

This dissertation is organized as follows:

Chapter 1, the introduction, starts with the problem definition, discuss the motivation of this dissertation and then discuss the contribution of this dissertation which is presented in the rest of the dissertation.

Chapter 2 provides the necessary background for reviewing and discussing the conventional CMUT fabrication processes. Then, the method for accomplishing the desired research is proposed.

Chapter 3 presents the analytical methods to design CMUTs. Then, the fabrication process adopted for the fabrication of the proposed CMUT are discussed, and preliminary tests are demonstrated to examine the success of the process before further processing.

Chapter 4 presents the characterization results of the fabricated CMUT that include the power efficiency, resonance frequency, bandwidth, fractional bandwidth and sensitivity of the manufactured device.

Chapter 5 draws up the achievements and propose future directions.

This dissertation focuses on the the development of a CMUT fabrication process, the FEA modeling and theoretical calculations were required for performance evaluation of the developed CMUT. Those modeling and calculations are provided and discussed in the Appendices.

Appendix A discusses the Finite Element Analysis (FEA) modeling the CMUT pitch-catch analysis to calculate the pressure in the fluid column and the received sensitivity of the receiving CMUT.

Appendix B presents the study analyzing the squeeze film damping effect in the CMUT cavities with trapped air.

Chapter 2

Background

The advent of Capacitive Micromachined Ultrasonic Transducer (CMUT) provided a better source of airborne ultrasound transducer particularly in the MHz operating frequency range [1]. Later, CMUTs showed a huge bandwidth advantage over the piezoelectric transducers under immersion, which has further motivated the development of sealed cavity based CMUTs for immersion applications [42]. In comparison to the piezoelectric devices the transduction in CMUT is attained electrostatically. The main advantage of CMUT over piezoelectric transducers is that CMUTs have better electro-mechanical coupling and much larger fractional bandwidth. Furthermore, the availability of the micromachining technology makes it possible to be fabricate miniaturized and precise CMUTs. Further, with the MEMS technology CMUTs can be fabricated in arrays. Also, with the MEMS technology, the CMUTs can be integrated directly with the driving circuitry which further enhances the performance of the CMUTs. However, the fabrication process complexity, cost, yield and performance of CMUTs still pose practical limitations and the researchers are still contributing to optimize and utilize the micromachining fabrication, by leveraging the advantages.

In this chapter, we present background of the CMUT fabrication techniques. We begin with an overview of the existing fabrication techniques with a brief comparison among the techniques. Afterwards, we discuss the material selection for the reported CMUT fabrication technique.

2.1 CMUTs Fabrication Technologies

CMUTs are fabricated on a high-conductivity silicon substrate to eliminate the requirement of an additional bottom electrode. High conductivity is achieved by heavily doping the silicon wafers. The membrane is then suspended over the substrate with the help of insulating sidewalls, creating a shallow cavity gap. The top electrode is formed by depositing a metal layer on the top of the membrane. In the case of non-conducting or high resistivity substrates, an additional bottom electrode is deposited. Conventional methods are further subdivided into sacrificial layer under-etching and wafer bonding, which will be discussed in the following sections in detail.

2.1.1 Sacrificial Layer Release Process

Sacrificial release process is established as the first method for CMUT fabrication and has been under extensive development since its first introduction [1, 43, 44, 45, 46, 47]. In the sacrificial release process, surface micromachining technology is utilized to create the vacuum gap by under-etching a sacrificial layer between the diaphragm and the substrate. The cavity is then sealed to make the CMUT suitable for immersion applications [42]. A general sacrificial release process is illustrated in Figure 2.1. In CMUTs, the aim is to achieve a vibrating membrane over a sealed cavity. In the sacrificial release process, the process starts with depositing an insulation (such as Si_3N_4) layer over the silicon substrate. The insulation layer, which acts as an insulator during device operation, is also used as an etch stop during the sacrificial release process. In the following step, the CMUT sacrificial release pattern is grooved in the insulator layer. Afterwards, a sacrificial layer (such as chromium or SiO_2) is grown. The Sacrificial deposition is followed by the deposition of another Si_3N_4 layer. Subsequently, top electrode is patterned by depositing Cr/Au. A new layer of Si_3N_4 is then deposited to bury the electrodes. Sacrificial release etch holes are lithographically patterned, and subsequently etched by the use of RIE. Afterwards, the sacrificial under-etching and release steps are performed and finally, the etch holes are sealed and desired membrane thickness is achieved by coating another thick layer of Si_3N_4 .

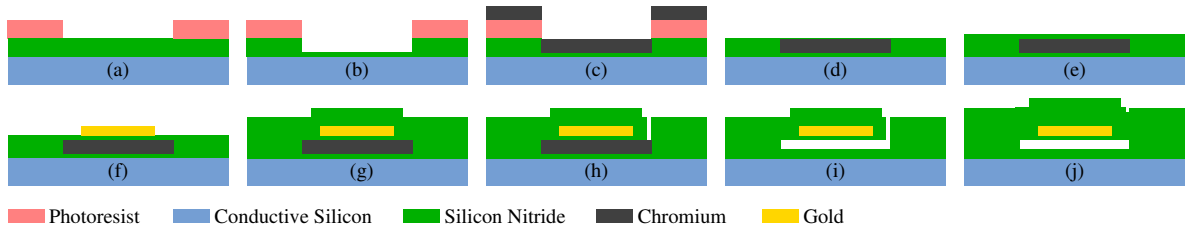


Figure 2.1: Process steps of the sacrificial release fabrication technique. (a) Image reversal lithography with sacrificial mask on insulating nitride; (b) DRIE defines the sacrificial cavity; (c) Chromium deposition into the sacrificial layer; (d) Liftoff and cleaning; (e) Membrane deposition; (f) Top electrode deposition; (g) Burying electrode under thick nitride; (h) Etch holes patterning; (i) Sacrificial under-etch and release; (j) Final cavity sealing. Reprinted from [48].

When fabricating CMUTs by adopting the sacrificial release process, a number of optimization adjustments needs to be made during design and fabrication steps, such as structural design, selection of membrane material, release holes position, selection of sacrificial material and relevant etchant type. Adjusting all of the design and fabrication steps is not practical. Moreover, obtaining a uniform gap height with the sacrificial underetching is quite challenging. Also, sacrificial release based CMUTs cause degradation in the device fill factor, due to the additional release holes for removing and releasing of the sacrificial layer [9]. With the increase of frequency the fill factor will decrease and, consequently, the output power and sensitivity decreases. Further, drying the cavity after wet underetching is another existing problem as stiction and collapse of membrane may occur during the process.

2.1.2 Wafer Bonding

At low operational frequencies, the radius of the CMUT increases and a uniform cavity height becomes more important. However, in these low frequencies and large-radius devices, sustaining the suspended membrane with the sacrificial release method is very difficult. Another way to fabricate CMUTs is the wafer bonding technique where two wafers are bonded together to fabricate CMUTs without the involvement of the

sacrificial layer underetching process. As a result, wafer bonding methods provide better control over the cavity formation and membrane thickness. Wafer bonding techniques do not involve the underetch process and combines surface micromachining and Silicon-on-Insulator for CMUTs fabrications [49]. Therefore, the wafer-bonding technique can also be adopted to address the membrane underetch stiction problems. Wafer bonding requires a pair of wafers: a prime wafer on which the cavity is defined and an SOI wafer carrying the device layer. After the cavity is patterned, the two wafers are brought into contact and bonded together. A very controlled cavity and uniform membrane thickness can be achieved with the wafer-bonding process [49, 50]. Wafer direct bonding, anodic bonding and polymer adhesive wafer bonding are the techniques reported in the literature and briefly discussed here.

Direct Wafer Bonding

Direct wafer bonding, in principle, relies on permanent covalent bonding [49, 51]. The bonding process is shown in Figure 2.2. An oxide layer under high temperature is grown on the prime wafer, which defines the cavity height. In the second step, the device structure is patterned on the oxide layer followed by a dry etch step to form the cavities. A thin layer of high quality oxide is then grown as an insulating layer which electrically isolates the substrate and top device layer. The prime wafer is then brought in contact with the SOI layer and a permanent covalent bond is established under very high temperature. In the subsequent steps, the handle and buried oxide (BOX) layers are etched leaving the device layer behind, which defines the membrane thickness. The device is formed at this stage, and the subsequent steps do not effect the cavity and membrane thickness. In the succeeding steps, the metalization for electrical contact and device isolation is carried out.

The main drawback of the SOI based direct wafer bonding is the high cost of SOI wafers and the equipment complexity associated with the production of high quality SOI. To overcome this complication a silicon nitride wafer can be bonded to the substrate wafer to form a SOI-free CMUT with direct wafer bonding [7].

Another disadvantage of direct wafer bonding is the high quality surface require-

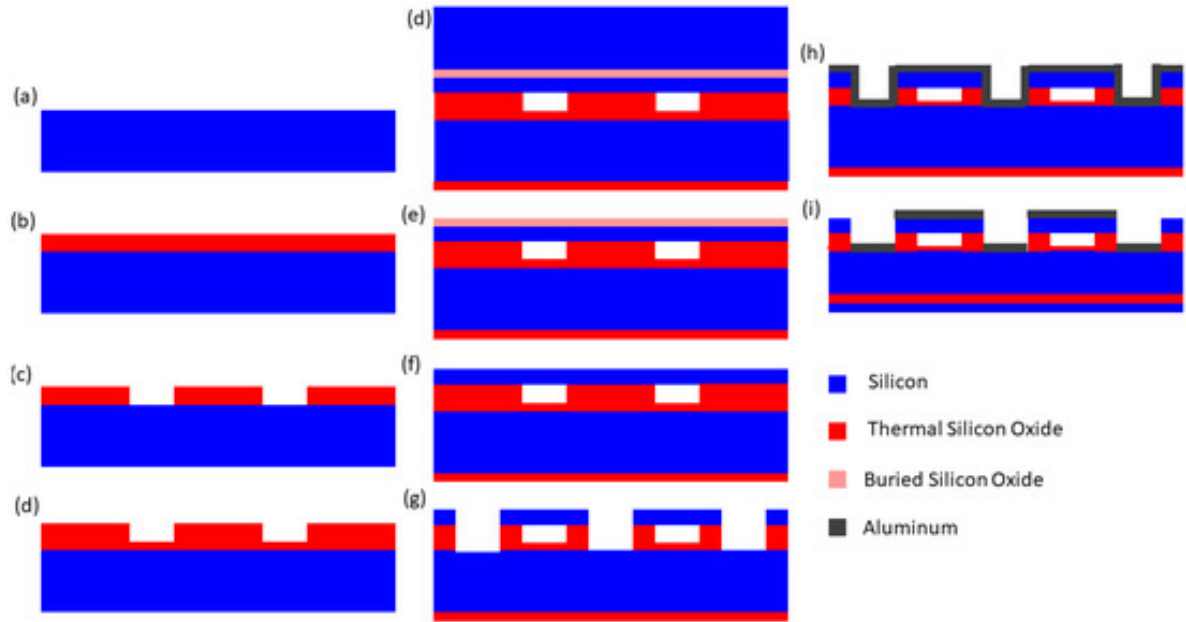


Figure 2.2: Process flow for direct wafer bonding CMUT. (a) Prime wafer; (b) Oxidation; (c) Cavity formation; (d) Thermal oxidation; (e) SOI wafer bonding; (f) SOI handle; (g) Removing BOX; (h) Metallization; (i) Electrode pattern and device isolation. Reprinted from [52].

ments, as it is high sensitive to cleanliness and roughness. The surface smoothness is generally achieved by either using an SOI wafer or apply surface treatment to such as chemical mechanical polishing (CMP) to non-SOI wafers [52, 7, 9]. The use of SOI wafers or CMP treatment can increase the yield but its makes the direct wafer bonding very expensive which is not desirable. Furthermore, the high temperature steps make it impossible to integrate the CMUT with the CMOS driving electronics.

Thermo-Compression Metal Bonding

A low cost low temperature thermocompression bonded CMUT with gold (Au) as intermediate layer was presented by Taklo et al. [53]. A silicon wafer and glass wafer pair was used to achieve a high strength and high bond yield. The cavity is defined on a silicon wafer with a KOH wet etch step. Then, a gold layer was sputtered into the structured silicon wafer. The same metal layer was sputtered deposited into the glass wafer. Next, the wafers were bonded manually with weak Van der Wall forces. After-

wards, the wafers to be bonded were placed in a lab-built thermo-compression bonder. A controlled pressure and a temperature of 450 °C was applied for 45 minutes. The sample temperature was gradually decreased before release of pressure and collection for further processing.

Recently, Li et al. [54], developed an SOI wafer based metal bonding process as illustrated in figure 2.3. The bonding process was carried out at 350 °C under a constant pressure of 80 kPa in an SB6 bonder.

Metal bonding is a low temperature process which is important for CMUT integration with the driving electronics. The major issue with the metallic bonded CMUTs is the electrical stability as the metal electrons may drift into the insulation layer when exposed to the bias voltage. Additionally, the use of SOI wafer rises the cost of the fabrication process which needs to be addressed.

Anodic Bonding

Anodic bonding is a wafer bonding process used to produce permanent seal between glass and silicon/metals wafers. Wafers are bonded in the presence of a high electric field [55, 56]. The glass wafer containing alkali ions is connected to the negative terminal, whereas silicon/metal gets connected to the positive terminal. The wafers to be bonded are placed in a heating chuck and temperature is increased to several hundred degrees after which an electrical potential of hundreds of volts is applied. The alkali ions which carry positive charge are attracted by the negative electrode and forms an ion depletion region at the interface. Oxygen ions move into the silicon surface when the electric field is applied and as a result forming of silicon dioxide to permanently bond the wafers.

The anodic bonding process has been reported for CMUT fabrication by many researchers [57, 58, 36]. The process illustrated in Figure 2.4 was reported by Yamaner et al [57]. Anodic bonding still utilize the device layer of the SOI wafer as the membrane, thus, the high cost problem still exists. Secondly, the bonding process requires an additional electric field step and hence add more complexity into the process. Furthermore, as the substrate is non-conducting, a bottom electrode needs to be patterned and insulated, which makes the process more complicated.

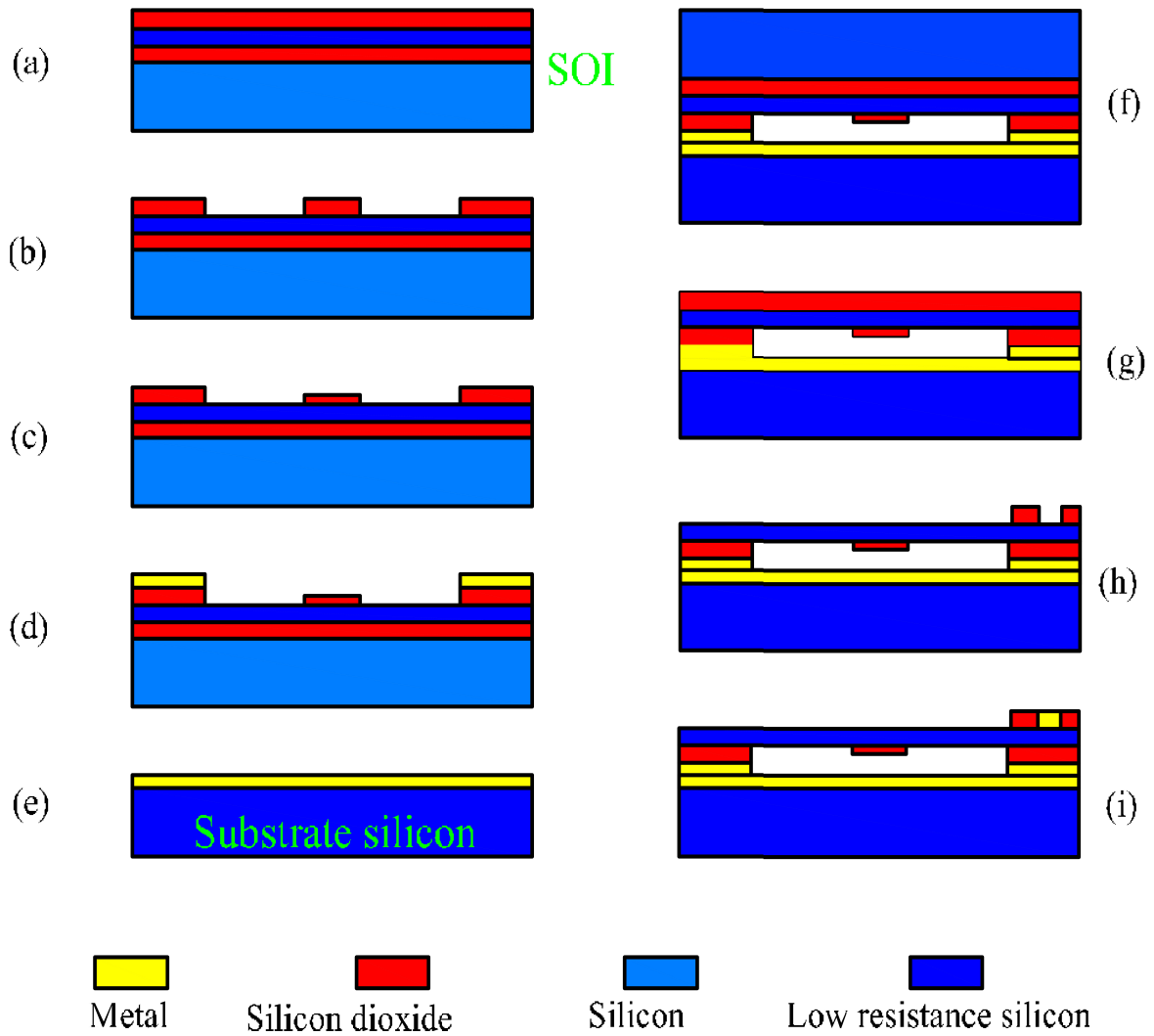


Figure 2.3: Metal-bonded CMUT process flow. (a) Oxidation; (b) Etching to form insulation layer; (c) Central insulation block; (d) Metal layer; (e) Metal layer on silicon wafer; (f) Wafer bonding; (g) Etching the handle silicon; (h) Etching the BOX; (i) Aluminum deposition and etching for metal pads. © 2015 IEEE [54].

Polymer Based Wafer Bonding

In recent years, researchers have been developing adhesive based wafer bonding for CMUT fabrication where the polymer adhesives are used as the bonding intermediate layer [10, 59]. The polymer adhesive in fluid form is first coated onto the wafers. Afterwards, wafers are pre-baked to cure the film before bonding. The wafers are then

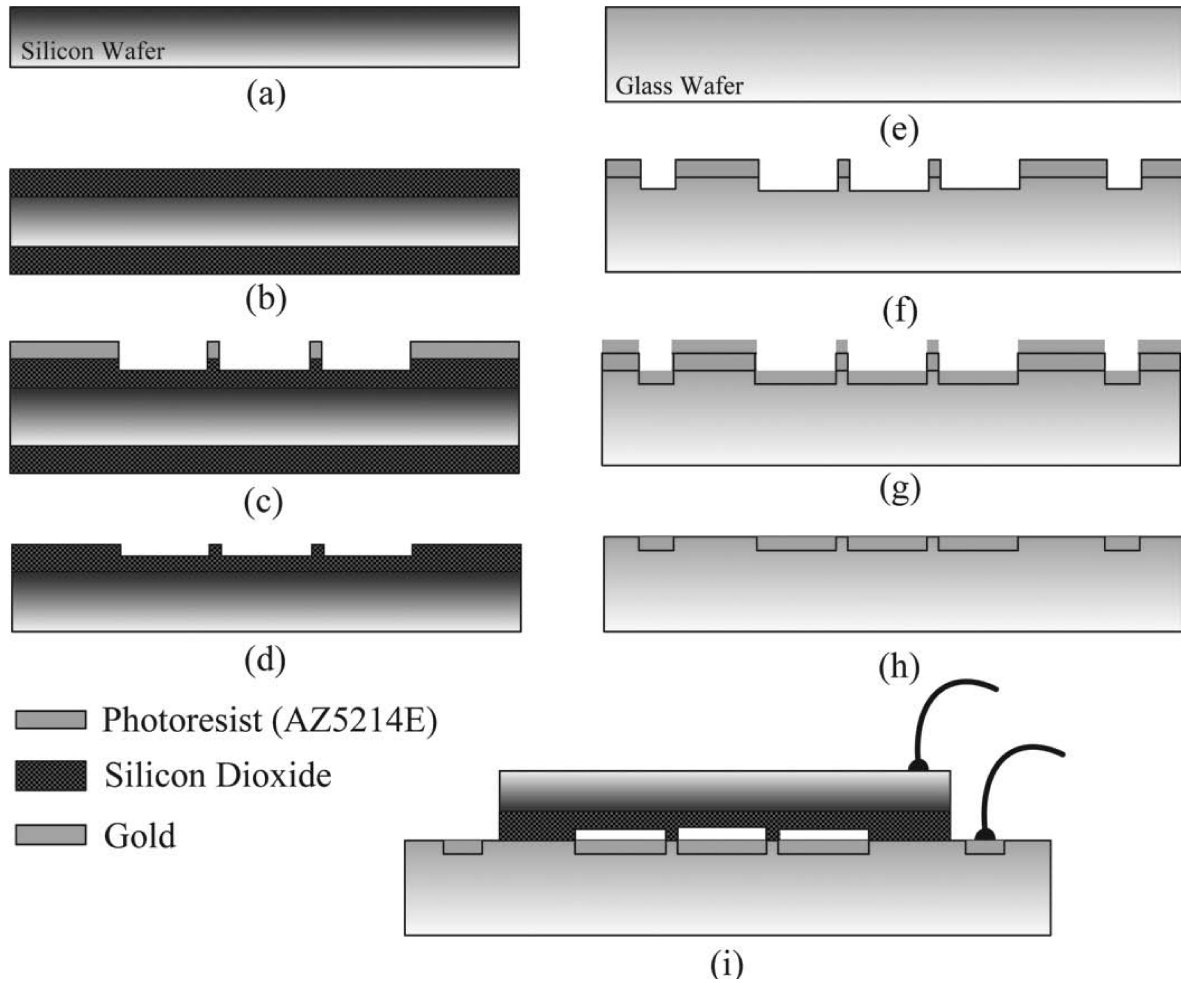


Figure 2.4: Anodic bonding process flow. (a-d) Thermal oxidation and oxide etching for cavity formation; (e-h) Etching glass, bottom electrode formation, and cleaning; (i) Anodic bonding. © 2012 IEEE [57].

brought in contact under thermocompression. A constant uniform force is applied under a constant temperature for some time and then the temperature is gradually decreased before release of the compression. Polymer adhesive based bonding has a number of advantages over the conventional wafer bonding. The wafers are coated with the adhesive in liquid form which, in turn, cover minor surface defects and surface contamination, thus minimizing high quality surface requirements. Secondly, adhesives have a high surface energy and low stress which results in low stress bonding. Thirdly, strong bonding force is attained at the bonding surface due to the large bonding area. Finally, adhesive based bonding techniques are low temperature processes which facilitates CMOS

integration. So far, SU-8 and Benzocyclobutene (BCB) adhesive polymers have been reported as adhesive intermediate layer for the CMUT fabrication [37, 38, 39, 60, 61, 62]. The processes reported for adhesive wafers bonding for CMUTs are still as complicated as the other reported conventional wafer bonding, as they either have used the costly SOI wafers [61] or glass wafers [60] which brings in the additional steps for electrode formation.

2.2 Selection of CMUT Fabrication Method

From the discussion about the different fabrication processes, the polymer adhesive based wafer-bonded technique appears to be a good choice for CMUT fabrication. It is much simpler and cost effective, has low equipment requirements, and provides higher yield. At the same time, adhesive bonding addresses some inherited problems discussed in Section 2.2.2.

2.2.1 Selection of Polymer adhesive for CMUT Fabrication

The first step in adhesive based CMUT fabrication is the selection of the adhesive material. Poly methyl methacrylate (PMMA) is a polymer which is commercially available and has been used in wafers bonding for other applications [63]. The proposed wafer bonding technique for the CMUT fabrication in this dissertation uses Poly methyl methacrylate (PMMA) adhesive as an intermediate layer for the thermocompression wafer bonding. The advantages associated with the PMMA adhesive based wafer bonding over other methods include low process temperature (usually 200 °C or less), high wafer surface defects and contamination tolerance, high surface energy and low bonding stresses. These factors will add cost effectiveness and simplicity to the CMUTs fabrication process.

2.2.2 Advantages and Disadvantages of Polymer Bonding

The accuracy control of the adhesive layer depends on the properties of the adhesive material. The properties of the adhesive materials are highly influenced by the thickness of the coating and the applied temperature during the spin coating and curing steps. The thickness of the coated adhesive polymers varies from hundreds of nm to micrometers. The thickness of the final adhesive layer depends on the material thickness and the spin speed [64, 65]. The desired thickness can be achieved by adjusting the acceleration and final speed of the spinner.

One of the major concerns associated with the adhesive materials is the lack of resistance to high temperatures and some chemicals during wet processing. For example, the PMMA has a melting point of 160 °C and become liquid at this temperature which may lead to the deformation of the pattern and/or un-bonding of the wafers. Besides that, the PMMA doesn't show any resistance to several chemicals such as acetone, toluene, hydrochloric acid, sulfuric acid and acetic acid etc. and easily dissolves in these chemicals [66].

Despite the limitation of the polymer adhesive, the advantages of the polymeric materials should be taken into consideration as well. Polymers are highly flexible in the coating, modification in the patterns and properties and so on. Materials such as Fillers can be mixed in the polymer matrix to get the original properties in the polymer matrix [67, 68]. Furthermore, the polymer can be optimally diluted to get some control in the thickness. Besides, the limitations of polymers are not permanent and they do promise a nice potential for optimization in specific applications.

Chapter 3

Design and Fabrication

In this chapter, we describe the design, manufacturing and testing of a PMMA adhesive based CMUT, intended for underwater acoustic applications.

3.1 Design of CMUTs

3.1.1 Design Methodology

The key parameters of the CMUT are determined based on the final application of the transducer. The design parameters like the radius and thickness of the membrane and the cavity height are defined based on the operational frequency and the collapse voltage. Further, the bandwidth, output pressure and receive sensitivity depends on these parameters. The radius, thickness and mechanical properties like, Young's modulus and Poisson ratio of the membrane defines the operational frequency. The collapse voltage of the CMUT depends on the cavity height and the membrane thickness, while the generated output pressure depends on the cavity height. The higher the cavity, the greater is the output pressure because of the greater membrane plate deflection, at the cost of higher collapse voltage. The CMUTs have better receive sensitivity for lower cavity gaps so the optimal cavity height needs to be chosen in order to operate the CMUT in both receive and transmit mode. The design process, the approximate geometry and fabrication process is initially determined using analytical expressions and an equivalent lumped circuit model for the CMUT. After the initial parameters calcu-

lations, the geometry can be optimized and modified as per device targeted operation using FEA methods. Subsequently, the finalized design is fabricated and characterized. Finally, the design parameters are verified by comparing the analytical results with the device experimental characterization results.

3.1.2 Analytical Modeling

Using the analytical expressions is a fast process to get the initial parametric values of the design. These value provide a good starting point for the CMUT lumped circuit model and the FEA model [69].

The resonance frequency of the CMUT is the primary objective of the design; all other parameters are optimized according to the operating frequency to get the desired input and output sensitivities. Equation 3.1 gives the center frequency of a CMUT operated in vacuum

$$\omega_0 = \frac{2.95 \times t_m}{a^2} \times \sqrt{\frac{E}{\rho(1 - \nu^2)}} \quad (3.1)$$

where t_m , a , E , ρ , and ν are the thickness of the membrane, the radius, the Young's modulus, density and the Poisson's ratio of the membrane material, respectively. Yet another parameter of interest is the collapse voltage, which is defined as the voltage at which the attraction force between the two plates overcomes the restoring force, and the membrane collapses to the substrate. The collapse voltage depends on the radius and thickness of the membrane, as well as the cavity height and can be expressed as follows:

$$V_c = \frac{1.56}{a^2} \sqrt{\frac{E \times t_m^3 \times g_0^3}{\epsilon_0(1 - \nu^2)}} \quad (3.2)$$

The cavity height in terms of collapse voltage can be obtained by re-arranging the Equation 3.2.

$$g_0 = 1.87 \left(\frac{\epsilon_0 V_c^2}{R_{rad} Q \omega_0} \right)^{1/3} \quad (3.3)$$

The cavity height plays a vital role in the performance of the CMUT and define the maximum allowable deflection of the membrane. The deflection in turn determine the output pressure and the input sensitivity of the CMUTs. The cavity height and membrane deflections are generally small in comparison to the membrane thickness. For calculating the deflection of a circular CMUT the spring-mass equivalent model can be adopted [69]. The corresponding spring constant and mass of the membrane plate can be obtained using Equation 3.4 and 3.5.

$$k_1 = \frac{192\pi D}{a^2} = \frac{16\pi Et^3}{a^2(1-\nu^2)} \quad (3.4)$$

$$m = 1.84\pi a^2 \rho t \quad (3.5)$$

In the underwater acoustic applications the ultrasonic transducers have the operational frequency in the range of 100 kHz–2 MHz [70]. The proposed transducer, in this dissertation, is intended to be used for underwater communication purpose in a commercial high-data-rate acoustic-modem, thus 200 kHz is opted to be the operating frequency. In receive mode, the transducer SNR improves with membrane weight [71]. As the intended use of the transducer is reception, the entire thickness of a 525 μm thick, heavily doped high-conductive silicon wafer was used as the suspended membrane. This also simplified the process as no further thinning steps were required. Based on the desired operating frequency and membrane thickness, the transducer radius was calculated to be 2.5 mm using Equation 3.1.

In receive mode a small cavity height provide better input sensitivity [72]. The cavity height is limited by the inherited waviness of the wafer surface and cannot be reduced indefinitely. An arbitrary gap height of 800 nm is considered and the devices are found to be functional at the considered height. The collapse voltage based on the

considered gap height of 800 nm and the radius and thickness of the silicon membrane was calculated to be 440 V using Equation 3.2.

Finally, the deflection of the plate along each point has been formulated as a function of the radial position as shown in Equation 3.6, where P_0 is the applied pressure on membrane plate as a result of the electrostatic force and the external ambient pressure. The membrane deflection under different pressure levels was calculated using Equation 3.6 as shown in Figure 3.1.

$$w(r) = \frac{P_0 a^4}{64D} \left(1 - \frac{r^2}{a^2}\right)^2 \quad (3.6)$$

The plotted deflection data shows that the central deflection is around 325 nm against the pressure of 9 atm. This deflection of 325 nm is well below the cavity gap height of 800 nm, therefore, the CMUT can easily be operated as deep as 100 meters under the sea level.

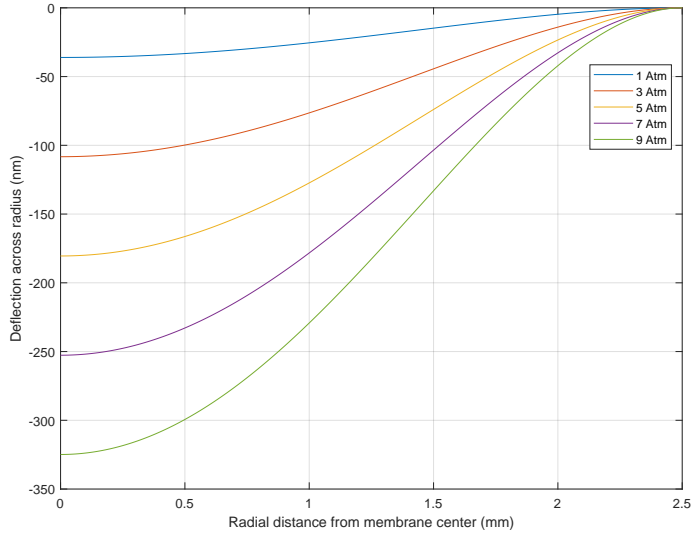


Figure 3.1: Effect on membrane deflection against membrane radial position for different ambient pressure levels.

The final fabricated and tested proposed device is a single-element CMUT consist of 16-cell as shown in Figure 3.2.

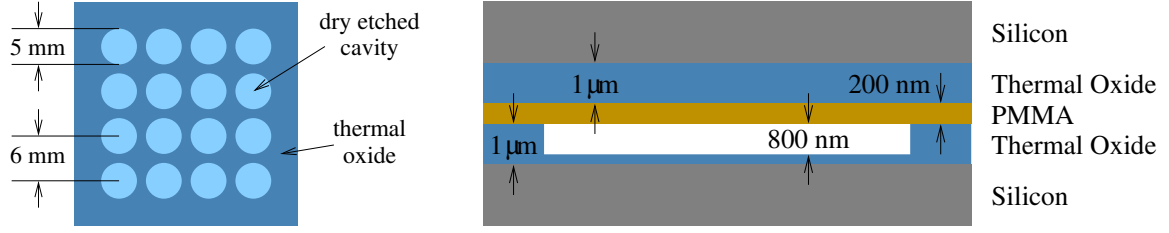


Figure 3.2: Top (**left**) and cross-sectional (**right**) views of the proposed Capacity Micromachined Ultrasonic Transducer (CMUT), showing device dimensions. Reprinted from [73].

The top view of the the 16-cells element and cross-sectional view of the CMUT single cell of the final device are illustrated in Figure 3.2. As the device was constructed using wafer bonding, extreme radius to cavity height ratios were feasible. A thermally grown silicon dioxide (SiO_2) layer was used as the cavity formation and insulating layer. The device cavity was formed in one of the bonding wafers by etching the SiO_2 using dry etching technique. Afterwards, the cavity carrying wafer is brought into contact with a PMMA spin coated second wafer. The highly-conductive wafers forming the two electrodes of the device were electrically isolated by the thermal oxide.

The summary of the parameters for the fabrication and the subsequent analysis is provided in Table 3.1.

3.2 Fabrication of CMUTs

The proposed CMUTs were fabricated using thermo-compression wafer bonding with PMMA adhesive as the bonding medium. A single mask was used to mark and print the geometrical structure into the substrate wafer in the fabrication process. The fabrication steps and operating conditions has been discussed in this section in details and conceptual sketches have been provided for better visualization.

Table 3.1: CMUT design Parameters

Parameter	Description	Value
a	Membrane radius	2.5 mm
t_m	Membrane thickness	525 μm
t_g	Cavity height	800 nm
t_i	Insulating layer thickness	1 μm
t_{pmma}	Adhesive layer thickness	200 nm
d	Distance between two cells	1 mm
f_0	Resonant frequency	200 kHz
V_c	Collapse voltage	440 V
V_b	Bias voltage	136 V

3.2.1 Mask Preparation

The fabrication process of the proposed CMUT has been carried out by using a single mask, single lithography step. A mask containing four elements where each element consist of 16 cells was drawn using a generic graphics application. The large radius size of the cells made it possible to use conventional lithography for mask preparation, thus avoiding e-beam lithography.

The photomask fabrication incorporate the same photoresist steps as the standard silicon substrate patterning processes. The mask is fabricated on a 150 mm \times 150 mm large and 2.3 mm thick bank quartz glass. A layer of pure chromium of 200 nm is evaporated into the blank glass. The designed CMUT pattern is printed into an acetate sheet to use as a dummy mask.

Photoresist is coated into the chromium deposited photomask. The pattern is then featured on the resist coated photomask by using the acetate mask while exposing the photomask to UV radiation. Subsequently, the exposed photomask is developed in a base developer. Lastly, the chromium layer is etched using chromium etchant leaving behind the patterned features, thus the pattern is transferred from acetate sheet into the chromium layer on the quartz glass. The dummy acetate mask and the final mask

are shown in Figure 3.3.

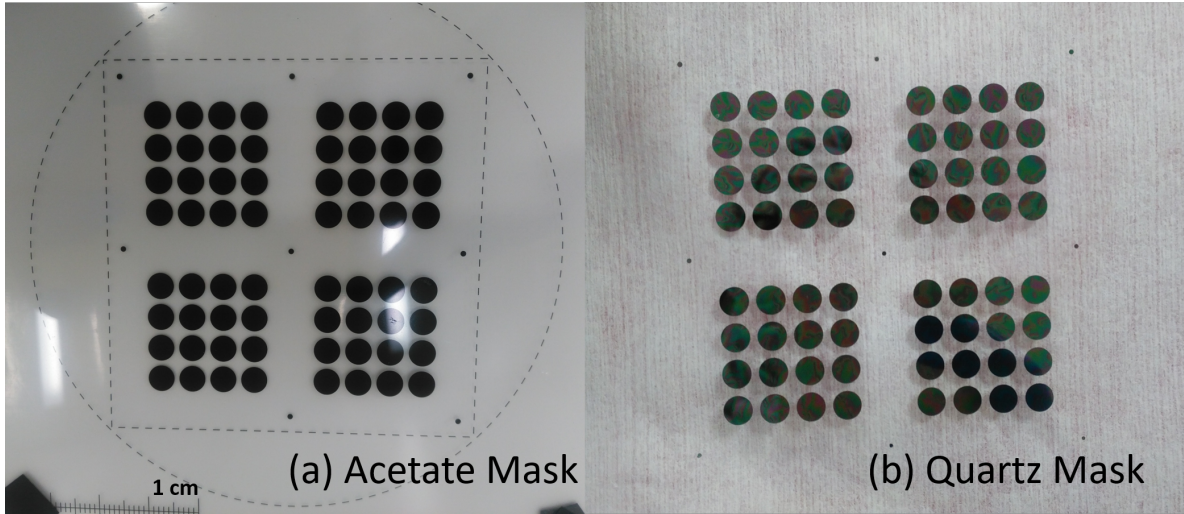


Figure 3.3: Photo mask. (a) The acetate mask used in lithography process to produce the final mask; (b) The final quartz mask.

3.2.2 Micro-Machining Steps

The micromachining process has been carried out in a class 1000 clean-room facility of Sabanci University Nanotechnology Research and Application Center (SUNUM). The process steps are thoroughly discussed in the subsequent sections.

Wafer Cleaning

Before any process, the cleaning of the wafer surface is necessary to remove and clean any dust or other contamination on the surface. The silicon dioxide wafer has been cleaned with acetone and isopropyl alcohol. First the wafer was kept in acetone for 5 minutes under temperature of 70°C . The acetone treating step is followed by an immediate isopropyl alcohol cleaning step as the acetone may leave a residue and form streaks on the surface when it evaporates. Thus, the wafer has been kept in the isopropyl alcohol for 10 minutes. After this step, the wafer is cleansed with DI water and dried with Nitrogen gun. Finally, the wafer has been soft baked for 15 minutes at 135°C to remove any residual water vapours and then kept at room temperature for half an hour to cool it down before further processing.

Photolithography

The structure and shape of the CMUTs must be developed to etch the silicon or the dielectric and develop the cavity grooves. Image reversal lithography process was conducted for the structuring of the CMUTs. A thick layer of $2\mu\text{m}$ AZ5214 E photo resist (MicroChemicals GmbH (Ulm, Germany)) has been spin-coated on the top of a thin HMDS primer layer. The photoresist was soft-baked for 120 seconds at 90°C . Subsequently, the photolithography step is carried out by exposing the wafer to ultra-violet (UV) light of $190\text{ mJ}\cdot\text{cm}^{-2}$ energy using Midas/MDA-60MS mask aligner. Post exposure the sample was soft-baked for 120 seconds at 115°C and then flood-exposed at $425\text{ mJ}\cdot\text{cm}^{-2}$. The sample was kept for 5 min at room temperature, and the final pattern was then developed in AZ 726 MIF (MicroChem) developer for 75 s. The lithography process is illustrated in Figure: 3.4 (a-c).

Silicon Oxide Etch

The silicon oxide from the patterned region has been DRIE (Deep reactive ion etch) etched using Oxford Plasma Lab 100 ICP300 RIE/ICP system. The oxide was etched using RF excited SF₆ gas for around 120 s to approximately etch 700–800 nm of oxide. The etching parameters are given in Table. 3.2. The remaining photoresist on the surface of the sample has been striped out by cleaning with acetone and isopropyl alcohol. The wafer was then treated with oxygen plasma using Torr Plasma Asher to remove any residual contamination. The oxide-layer etched wafer is shown in Figure: 3.4 (d).

PMMA Coating

Another silicon oxide wafer was thoroughly cleaned as discussed above in the wafer cleaning section. Afterwards, A PMMA layer [950 PMMA A4, MicroChem] is spun-coated to the silicon with a spin rate of 1000 rpm for 15 seconds and then 4000 rpm for 45 s to achieve a 200 nm thick PMMA layer on the oxide wafer. The PMMA layer needs to solidified to avoid fluid flow on the surface and also, to remove the nano bubbles

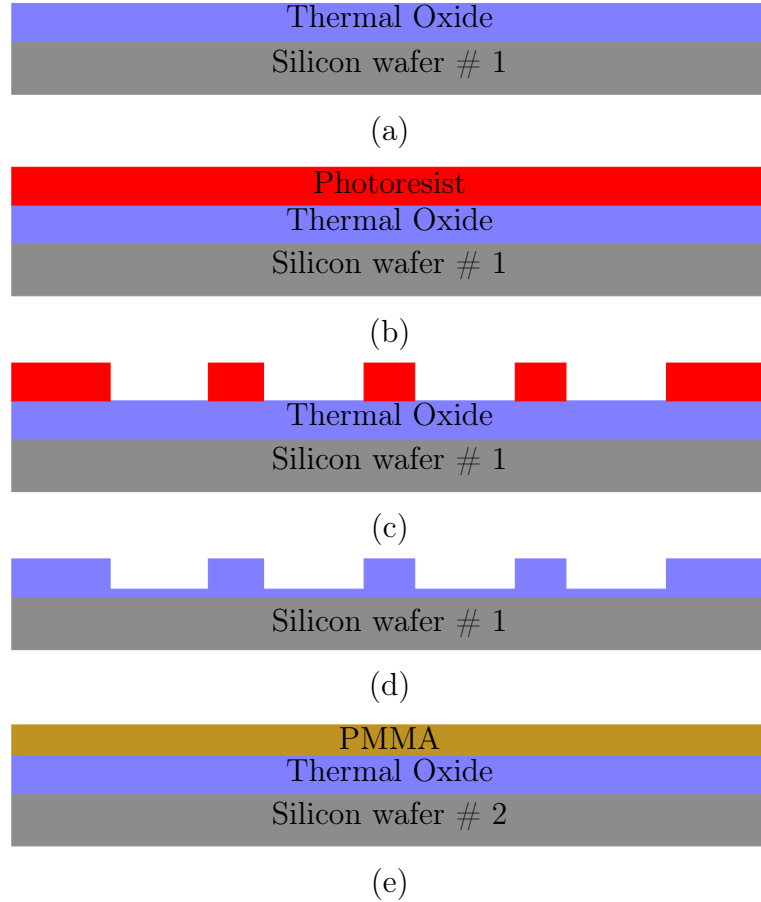


Figure 3.4: Surface Micro-machining steps for CMUT fabrication. (a) Thermally grown oxide wafer; (b) Spun coated photoresist; (c) CMUTs shape development using photolithography; (d) DRIE etched oxide layer for cavity formation; (e) PMMA spun coated second oxide wafer.

that may have formed on the surface layer. Therefore, before bonding the PMMA was annealed at 180°C for around 20 minutes to avoid bubble formation and remove any existing organic residuals. The final PMMA coated wafer is shown in Figure: 3.4 (e).

3.2.3 Wafers Thermocompression Bonding

The PMMA coated and the cavity carrying wafers facing each other were then and carefully aligned for the final bonding. Before placing the sample in the bonding chamber the wafers to be bonded were wrapped in an aluminum (Al) sheet to avoid chances of

Table 3.2: Silicon Dioxide Etching Parameters

Parameter	Value
SF ₆ Flow Rate	45 sccm
Chamber Pressure	7.5×10^{-9} Torr
SF ₆ Purging at	15×10^{-3} Torr
DC Power	50 W
RF Power	2000 W
Table Temperature	200 °C
Etch Rate	2.5 nm/sec

any contamination. Another advantage the Aluminum sheets offers is the assistance in uniform distribution of the pressure along the surface during the thermo-compression bonding process. The wafers were then deposited into the lab-built thermocompression bonding tool for bonding purpose. The Thermocompression bonder and the wafer bonding setup is discussed in Section 3.3 in details. The whole fabrication process is summarized and illustrated in Figure: 3.5

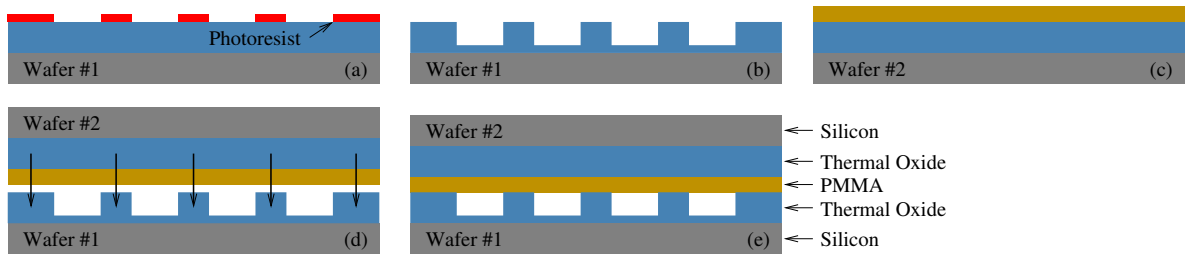


Figure 3.5: Process steps for CMUT fabrication. (a) Pattern lithography and developing; (b) Oxide etching and cleaning; (c) Polymethyl methacrylate (PMMA) coating; (d) Membrane and cavity alignment and bonding; (e) Final structure. Reprinted from [73].

3.3 Thermocompression Bonder

The thermocompression bonding setup in question is engineered to simplicity, at the laboratory of the Sabanci University Acoustics Group (SU-Acoustics), using the available equipment in the laboratory. The parts of the entire setup is labeled and illustrated in Figure 3.6. The main bonding chamber is constructed with an inverted glass desiccator. The entire chamber rests on a steel pipe bent in the form of a circle which is supported by 4 aluminum legs fixed on a wooden base. A heat insulating ceramic plate supports an aluminum fixture. which forms the footing for the bonding elements as displayed in Figure 3.7. On the top of the fixture are four springs for back support during compression. The black screw (marked as "A" in Figure 3.7) acts as the compression element and we call it the "Compression Screw". The electrical configuration of the system are depicted in the schematic representation of Fig. 3.6. The heaters are driven by a PID temperature controller. Vacuum is created with a rotary pump and monitored by a pressure gauge connected to the main chamber.

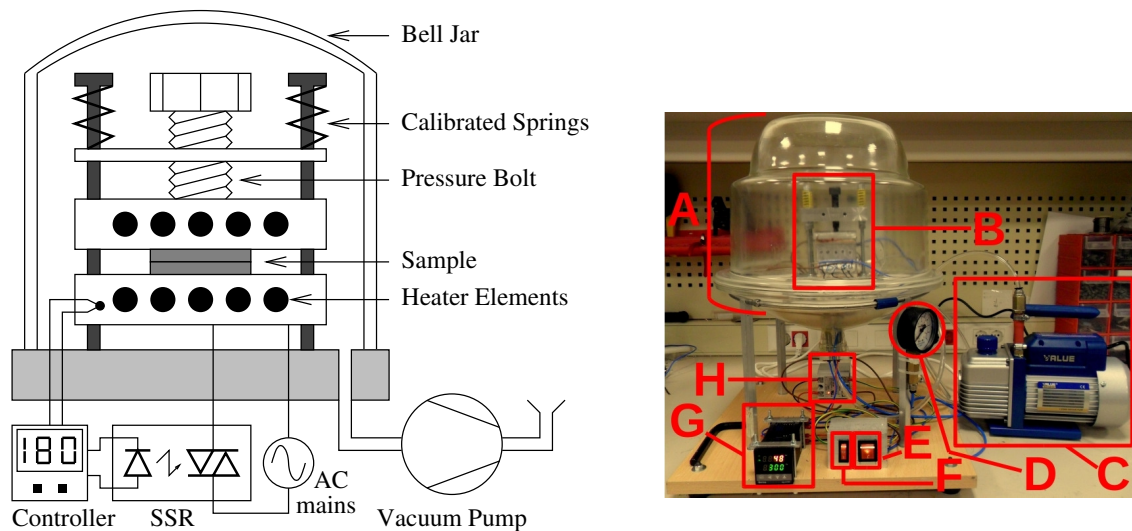


Figure 3.6: The developed thermocompression bonder. Schematic (left). Actual (right) Thermocompression bonder setup. (A) Bonding chamber made of inverted desiccator; (B) Bonding element and fixture inside; (C) Pump; (D) Vacuum Gauge; (E) Main power; (F) Heater power; (G) Temperature controller; (H) Relay. Reprinted from [73].

The bonding elements are separately exhibited in Figure 3.8. The top aluminum

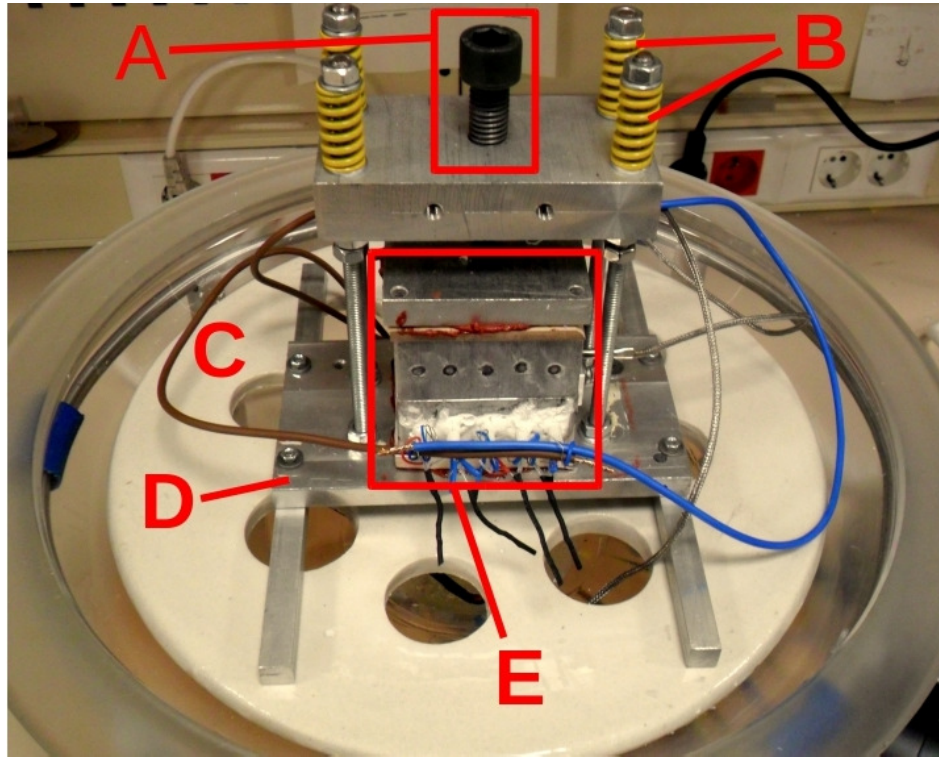


Figure 3.7: Embodiments inside the chamber. (A) Compression screw; (B) Support springs; (C) Supporting ceramic plate; (D) Aluminium fixture for bonding elements; (E) Bonding elements (Thermal and compression).

slab ($6\text{ cm} \times 6\text{ cm} \times 1\text{ cm}$), metal ball (7 mm in diameter) along with the compression screw forms the compression elements. The compression elements are insulated from the heating elements by a ceramic slab ($6\text{ m} \times 6\text{ cm} \times 0.6\text{ cm}$) adhered to the aluminum slab. The heating elements are manufactured with two blocks of aluminum. Each block has the dimension of $6\text{ cm} \times 6\text{ cm} \times 2.5\text{ cm}$. Five heater elements (24V 50W A1322 soldering station replacement heating element ceramic heaters) are inserted into each aluminum block and sealed with white cement as shown in Figure 3.8(C). The heating elements are insulated again from the aluminum fixture footing below by another ceramic slab.

Temperature sensing is performed by a thermocouple connected to the heating elements from the side of the bonding interface. The pressure gauge calve, pump pipe,

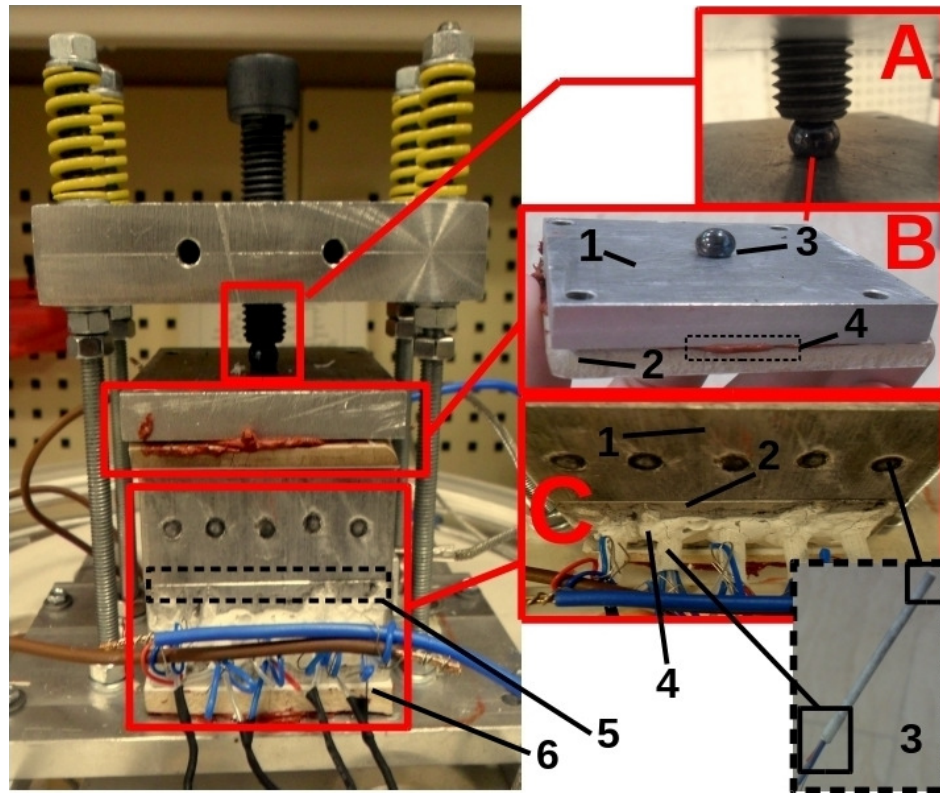


Figure 3.8: Bonder elements. (A) Compression contact; (B) Compression element. (1) Aluminium slab; (2) Thermally insulating ceramic slab; (3) Compression contact ball; (4) Ceramic to aluminium adhesion composite; (C) Thermal elements. (1) Upper Aluminium block; (2) Lower Aluminium block; (3) The heating elements (5 are inserted into the upper Aluminium block and 5 into the lower); (4) Holes with the heater are sealed with white cement; (5) Bond interface; (6) Thermally insulating ceramic slab between thermal element and Aluminium fixture.

thermocouple connection and the electric wires are passed through the opening of the desiccator lid and then sealed with two-part epoxy. Parts of the setup are displayed and labeled in Figure 3.9.

Pressure calibration for bonding is done using a load cell (Figure 3.10). The device is inserted to the aluminum fixture and the compression screw is turned to get an electrical voltage measurement. Evaluation yields that one full turn of the compression

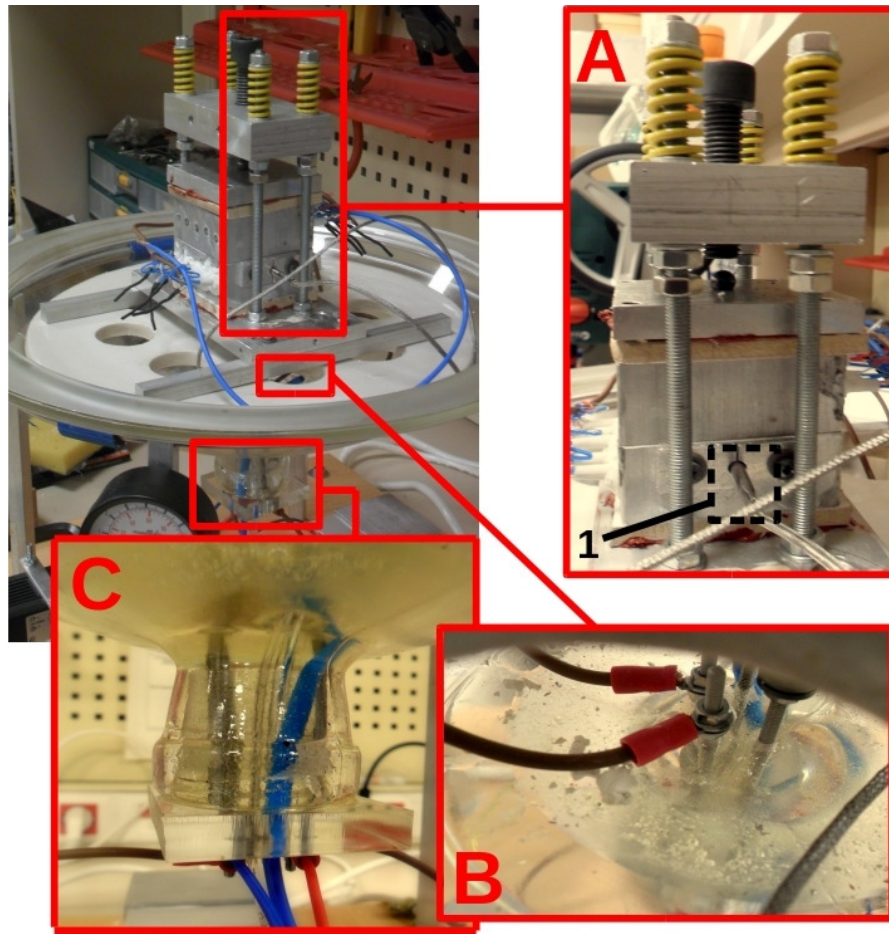


Figure 3.9: Side-view displaying the (A) (1) Thermocouple; and (B)-(C) Epoxy sealed duct for wire passage.

screw yields 40 kilogram weight. For the experiments we have used 20 kilogram weight for compression which correspond to 0.5 turns of the compression screw.

3.3.1 Wafer Bonding Process

For bonding purposes, the Al-wrapped wafers (as discussed in section 3.2.3) are placed in the thermocompression bonding unit. Next, a pressure is applied by the compression element with the help of the compression screws. To determine a feasible bonding pressure, several experiments are performed by gradually increasing the pressure in



Figure 3.10: Manufactured cantilever for compression force calibration.

each step. The main concerns during the pressure calculation for bonding are the PMMA deformation under compression and wafer sample breakdown. Therefore the aim is to apply a minimum possible pressure to get a strong enough bond between the wafers. Consequently, A pressures of 435 kPa is found to be sufficient, pressure values below were found to be insufficient for bonding and pressure levels above 435 kPa were avoided to reduce the possibilities of PMMA deformation. After applying the pressure the chamber was evacuated before turning the heating unit on.

In the next step, the temperature is gradually raised to 180 °C. For 60 minutes of a constant pressure and temperature, the wafers are kept compressed together for the bonding. After the bonding process, the temperature is gradually decreased to 30 °C by turning the heat off, before the pressure and the vacuum has been released. Finally,

the manufactured device is collected and prepared for packaging, characterization, and testing.

3.4 Preliminary Testing and Packaging

Before the packaging of the bonded device, the CMUT bond was initially evaluated by applying an alternate current (AC) signal in the audible range and the bonding of the buzzing CMUTs are declared as successful. The CMUT was then fixed on an aluminum slab which is used as the device handle and also as a backing layer. Silver epoxy was used for the fixing purposes which provide electrical conductivity and make it possible to provide the electrical connectivity to one of the electrodes from the back. The second electrode is connected to the top wafer using silver epoxy. The CMUT carrier slab is then mounted on an aluminum rod which operates as handling arm in the experimental and characterization phase. The ready to bond CMUT cavity in the fabrication stage, the final packaged device, and the schematic of the final device are shown in figure 3.11

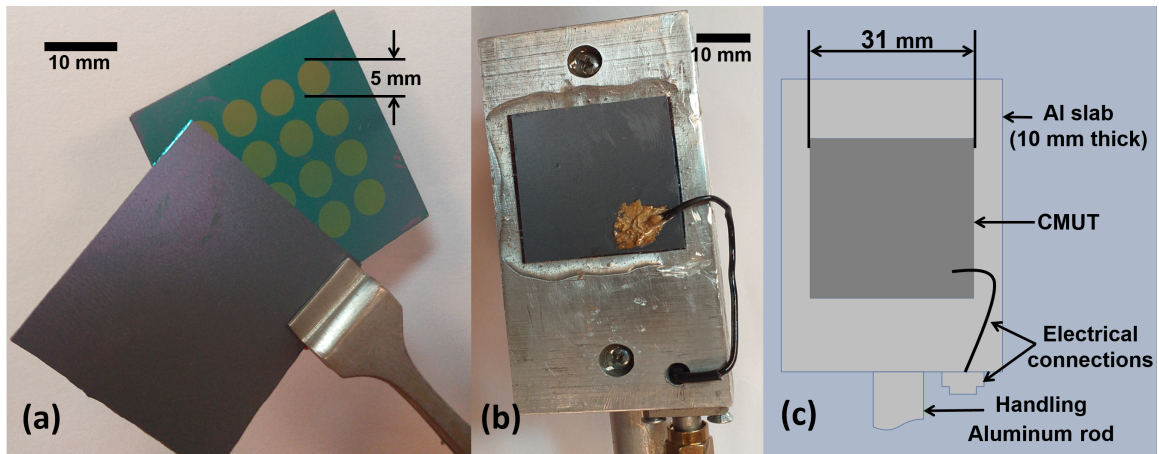


Figure 3.11: Device during fabrication stages. (a) Before bonding; (b) Final device; (c) Schematic of the final device. Reprinted from [73].

3.5 Bonding Quality

The bonding quality was evaluated by dicing the bonded wafers into small squares of length 10mm each, where the stiction of the diced sample sustained. Additionally, the device showed consistency in the results when been operated for several hours over a period of few months, thus, the bonding is considered as successful.

3.6 Comparison of the Developed Fabrication Technique to the Existing Fabrication Techniques

The developed PMMA-based CMUTs are compared with the other published fabrication processes to assess their complexity, cost, equipment requirements, and flexibility.

System complexity is one of the comparison parameters. Wafer-bonding techniques are much simpler as compared to sacrificial-release fabrication methods, as the latter need a number of adjustments and selections such as alignment steps, choosing the proper etchant and materials for the sacrificial layer and membrane. Low-pressure chemical-vapor deposition silicon nitride (LPCVD SiN)-based wafer direct bonding needs CMP treatment. Anodic bonding needs an electric field during the bonding process that adds complexity to the process. SOI-wafer-based wafer direct bonding and adhesive bonding are considered simple, as they do not have additional bonding requirements.

Wafer cost is another comparison parameter, even though wafer cost is a very small fraction of the total when compared to clean-room equipment costs. However, the use of expensive SOI wafers in wafer-boding techniques makes wafer cost an important parameter.

The number of fabrication steps reflects equipment requirements and its usage costs. Furthermore, more fabrication steps also add to the chances of error, which depends on the efficiency of the used steps. It is therefore preferable to have fewer fabrication steps in order to avoid the mentioned problems.

Adhesive bonding techniques are flexible as compared to other methods. The other

fabrication methods are very strict in the selection of wafers and their surface smoothness.

The processes were evaluated based on material cost, temperature requirement, deposition and etching steps, lithography steps, system simplicity, and special bonding restrictions. The evaluation parameters are summarized in Table 3.3. According to the data, PMMA-based fabrication is simple and highly cost-effective.

Table 3.3: Comparison of fabrication methods.

Comparison Criteria	Fabrication Technique					
	Sacrificial Layer-Based [9]	Wafer Direct Bonding			Adhesive Bonding	
		SOI	Non-SOI	Anodic	Other	* PMMA
		Wafer-Based [51, 49]	Wafer-Based [7]	Bonding [58]	Methods [38, 37]	-Based [73]
Wafer pair	N/A	SOI Si	LPCVD SiN LPCVD SiN	SOI Si	LPCVD SiN Si	SiO ₂ SiO ₂
Wafer cost	low	high	low	high	low	low
Special requirements	N/A	N/A	CMP required	Electric field	BCB as adhesive	PMMA as adhesive
Surface-quality restriction	N/A	Restrict	Restrict	Restrict	low	low
Max Temp	785 °C	1100 °C	1000 °C	350 °C	240 °C	180 °C
Deposition required	yes	yes	yes	yes	yes	no *
# of lithography steps	5	4	3	3	3	1 *
# of wet etching steps	3	3	1	3	2	0 *
# of dry etching steps	4	2	2	1	2	1 *
Simplicity	low	high	high	low	high	highest

* The presented CMUT was specifically used for low frequencies. Higher frequencies can also be achieved at the cost of additional etching and metal-deposition steps as discussed earlier in Section 1.

Chapter 4

Characterization

In this chapter the detailed static and dynamic characterization of the fabricated CMUT are presented. The characterization involve the measurements of key static and dynamic parameters like, cavity depth, power efficiency, transient and steady state responses, electrostatic spring softening, sensitivity, output power, and bandwidth of the CMUT. The parametric values have been verified by comparing the measured results with the Finite Element Analysis (FEA) results. A very good agreement has been observed among the measured and simulated values.

4.1 Static Characterization

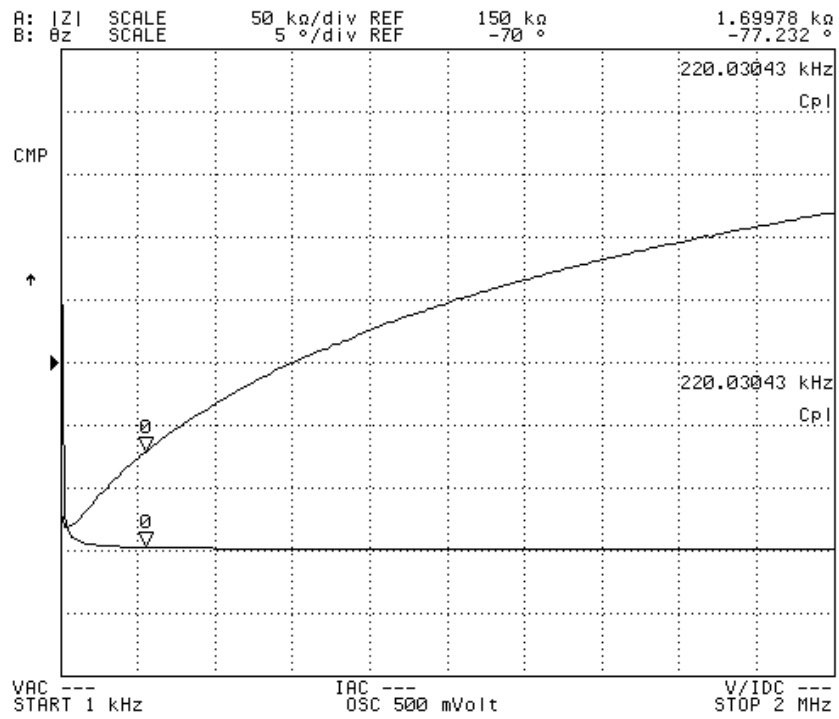
Static characterization have been carried out using impedance analyzer and optical profilometer. The static parameter measurements are briefly discussed in this section.

4.1.1 Impedance Analyzer Analysis

The impedance and its corresponding phase angle (ϕ) was measured using an impedance analyzer. The impedance analyzer measurements were performed without and with a 40 V DC bias. The biased and unbiased $|Z|$ and ϕ plots are shown in Figure 4.1. The plots show that the value of ϕ gets better upon applying a bias voltage which shows that the capacitive device have more radiation losses when biased and in turn improves the power efficiency of the CMUT. The power efficiency has a direct proportional relation

with the Cosine of ϕ as described in [74].

(a). $|Z|$ and ϕ without DC bias



(b). $|Z|$ and ϕ with 40 V DC bias

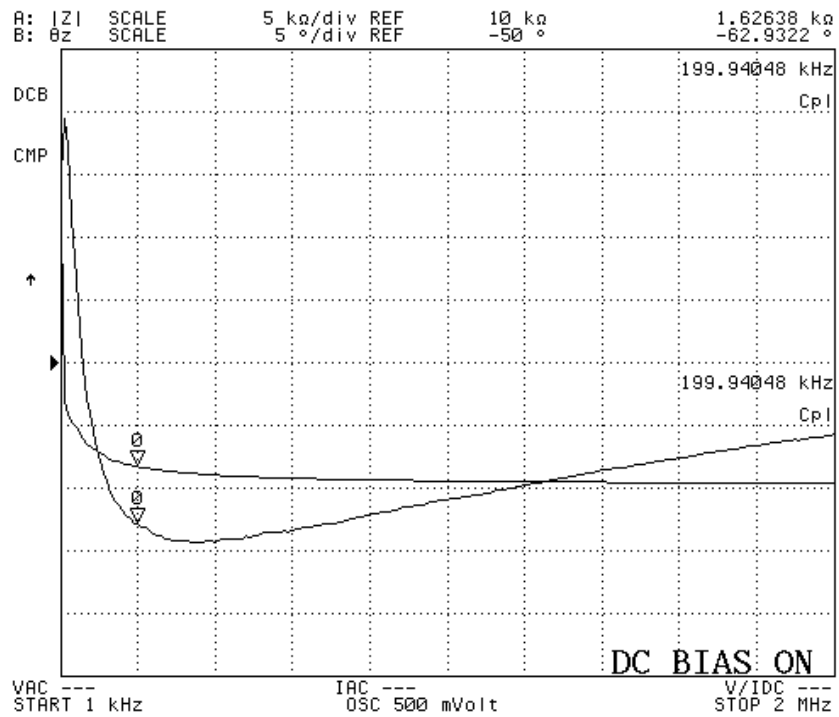


Figure 4.1: Impedance analyzer measurements

4.1.2 Optical Profilometer Analysis

The cavity depth of the oxide etched wafer and the spin coated PMMA thickness are measured before bonding using optical profilometer (STYLUS PROFILOMETER P-17, KLA - TENCOR). The pre-bonding cavity depth of the measured sample is found to be 580 nm, while the PMMA coating is 155 nm as shown in Figure 4.2.

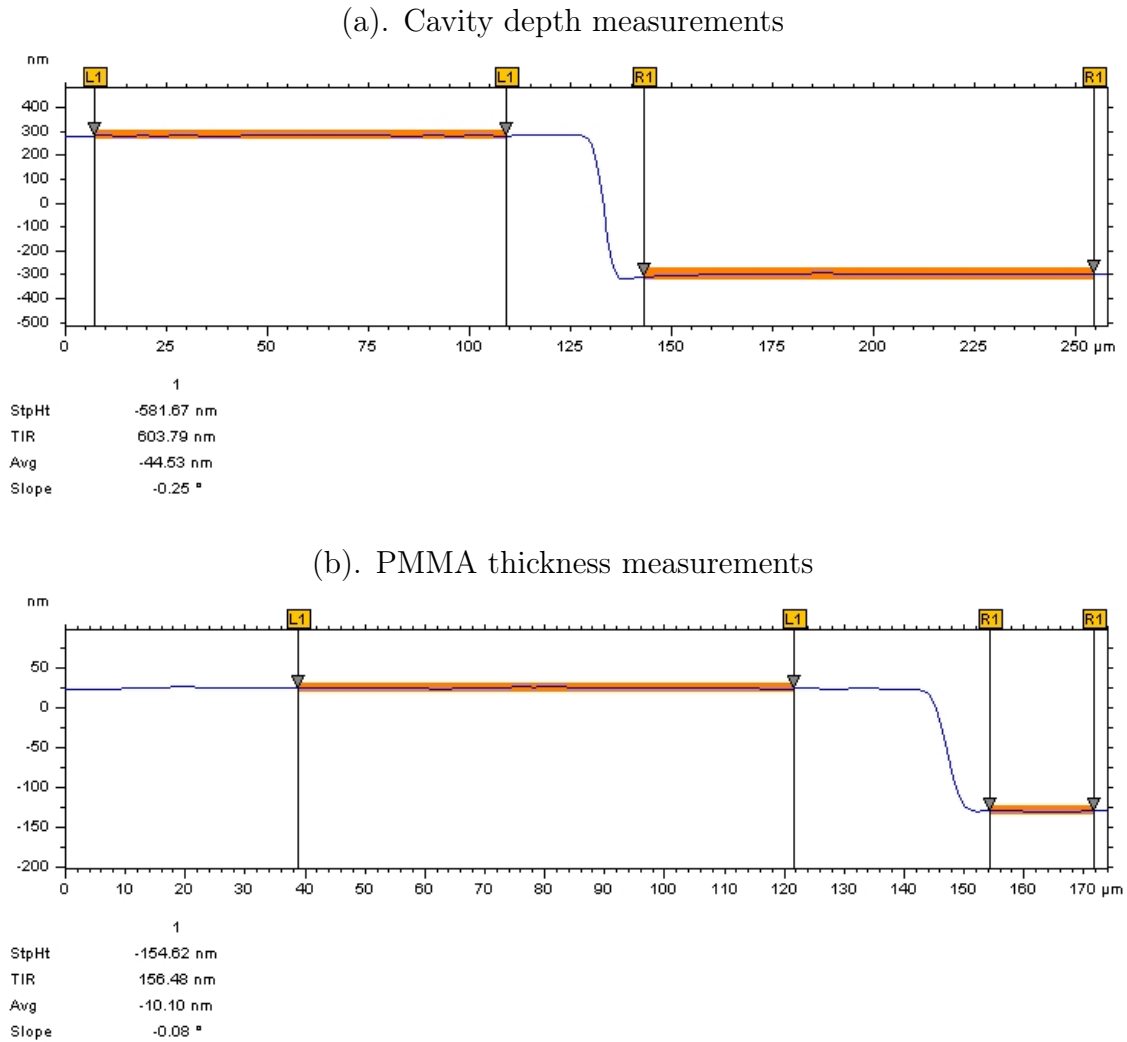
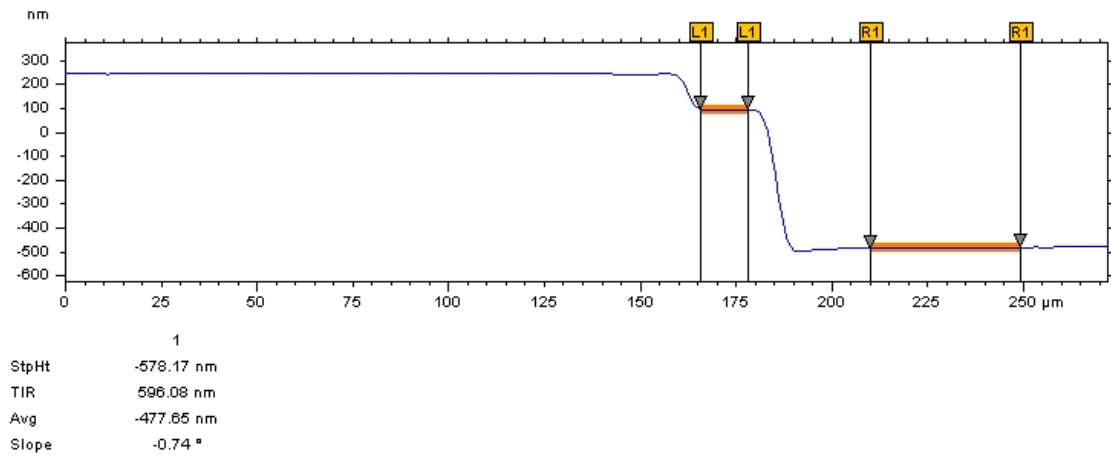


Figure 4.2: Pre-bonding optical profilometer measurements

To investigate the conduct of thermo-compression bonding on the PMMA deformation and in turn its effect on the cavity height, one of the bonded sample is un-bonded by applying a mechanical force. Upon inspection, it is found that some of the PMMA has stuck to the cavity carrying wafer while some of it remained it contact with the

PMMA coated wafer. The stiction to either one wafer or the other is due to the strong cohesive force among PMMA molecules. In a microscopic assessment it is found that the film PMMA has not flown into the cavity regions. The CMUT cells having PMMA around the cavity were again examined with the profilometer. Results shows that the cavity depth and the PMMA thickness are almost the same as before the bonding process as illustrated in Figure 4.3. Hence, it can be deduced that there has been no change in the cavity depth due to the adhesive bonding neither the thickness of the PMMA layer has significantly changed due to the thermocompression.

(a). Cavity depth measurements



(b). PMMA thickness measurements

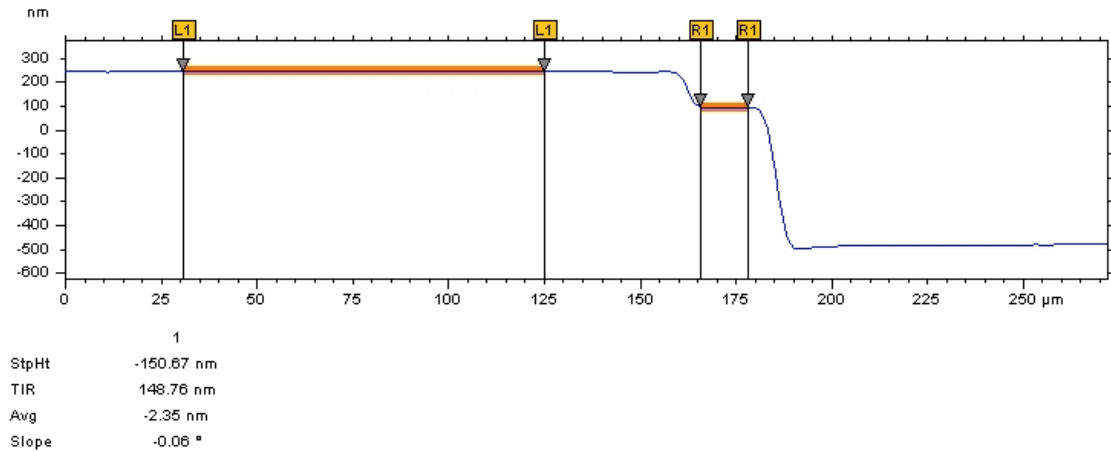


Figure 4.3: Post-bonding and un-bonding optical profilometer measurements

4.2 Dynamic Acoustic Characterization

The dynamic acoustic characterization of the fabricated CMUTs was carried out to determine the transmitting and receiving capabilities in immersion. As shown in Figure 4.4, a pitch-catch experiment was carried out in sunflower oil immersion to test the fabricated CMUTs. Sunflower oil was used as the medium to avoid electrical short circuit between the exposed electrodes while preserving acoustic properties closer to that of water [75, 76]. A pair of CMUTs fabricated under same condition on identical wafers were used for the acoustic characterization. Both CMUTs were immersed in the sunflower oil where one was used for generating the ultrasonic signal and called the transmit-CMUT (Tx-CMUT), while the other one, the receive-CMUT (Rx-CMUT), was receiving the ultrasound signal. The attenuation coefficient of sound in the sunflower oil is given by $\alpha = A.f^n$, where $A = 7.83 \times 10^{-12}$ and $n = 1.84$ while the speed of sound in the sunflower oil is calculated to be 1480 m/s [75, 76].

Both of the CMUTs were biased with 136 V, and a signal generator [Keysight 33250A (Santa Clara, CA, USA)] is used to drive the transmitting-CMUT (TX-CMUT) with a two-cycles $20 V_{pp}$ sine burst. The driving circuit consists of a bias resistor (R_{BIAS}) and a decoupling capacitor (C) having values of 100 k Ω and 100 nF, respectively. The receiving circuit was identical to the driving circuit, and the signal was captured using an oscilloscope [Keysight DSO-X 2014A (Santa Clara, CA, USA)] without any intermediate amplification.

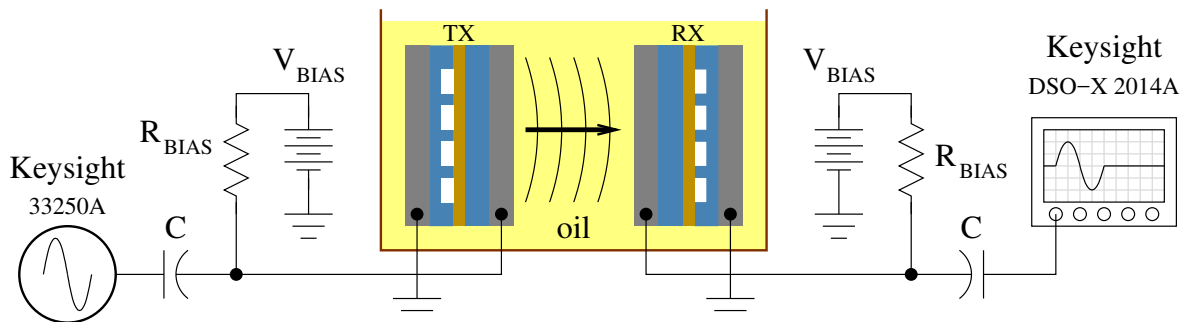


Figure 4.4: Setup for pitch-catch experiment. Reprinted from [73]

4.2.1 Bandwidth

To calculate the bandwidth (BW) of the fabricated CMUT, the frequency of the input AC signal was swept from 100 kHz to 300 kHz with an increment of 10 kHz. The peak amplitude of the acquired signal was recorded at every sweep point. In order to measure the output voltage at steady-state, a burst of 15 cycles was applied to the input of the transmitting-CMUT for every measurement. The signal received against an input sine burst at 200 kHz in time domain is shown in Figure 4.5 (left), while the plot on the right the normalized magnitude for the frequency sweep. The center frequency, f_{center} , is observed to be in the span of 190 kHz–200 kHz. The full-width at half-maximum bandwidth (FWHM-BW) of the device is found to be 66.4 kHz, which corresponds to a fractional bandwidth of 33.6%.

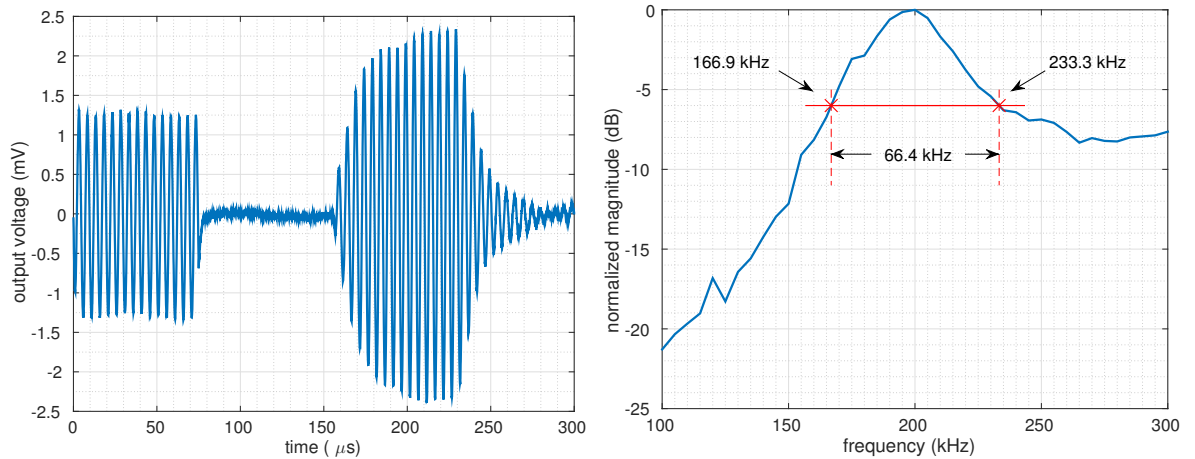


Figure 4.5: Output signal of RX-CMUT for a tone burst of 15 cycles at 200 kHz (**left**), normalized magnitude for a frequency sweep from 100 to 300 kHz (**right**). Reprinted from [73].

4.2.2 Sensitivity

The sensitivity of an ultrasonic device is the measure of output voltage against per unit applied input pressure and is often specified in $[V/Pa]$. In order to calculate the sensitivity of a CMUT, the applied input pressure must be known. The output pressure of the TX-CMUT was obtained analytically with the help of Finite-Element-Analysis

(FEA) model by matching the electrical measurements of the experimental results to the FEA model of the experimental set up. The FEA model was designed in ANSYS Multiphysics (V18.1, ANSYS, Inc., Canonsburg, PA, USA) and is described in details in Appendix A.

The designed electromechanical FEA model was completely mimicking the experimental conditions, the TX-CMUT is driven from the electrical port which electromechanically generates pressure in the fluid medium. The produced pressure was then sensed by the receiving-CMUT (RX-CMUT) and the output voltage is calculated in electrical conditions identical to that of the experiment. The device parameters were then tuned up to match the experimental results. The adjustable parameters were stiffness of the membrane material and the effective cavity gap as the gap height may change due to the waviness of the wafer surface. The simulation results showed the presence of a significant amount of damping in the experimental data. This was accounted to squeeze film damping, which can occur in CMUTs for large radius to cavity-height ratios and that ratio for the fabricated devices is 2.5 mm to 800 nm. To include the effect of the damping, viscous dampers were included to the FEA model Damping parameters were determined empirically to match the FEA results to the experimental data. The presence of the squeeze film damping was analyzed for the the manufactured device and the analysis is provided in Appendix B. Diffraction losses and absorption in the coupling fluid medium were not taken into the account due to the very small separation distance between the TX-CMUT and RX-CMUT.

The FEA result for output voltage of the RX-CMUT and the experimental output voltage are plotted in Figure 4.6. The corresponding acoustic pressure on the input of the RX-CMUT and in the fluid column was then obtained from the simulation results. A pressure of approximately 4 kPa_{pp} was found to be produced in the coupling fluid by the TX-CMUT when a two-cycles burst of 20 V_{pp} sine wave at 200 kHz is applied under 136 V DC bias.

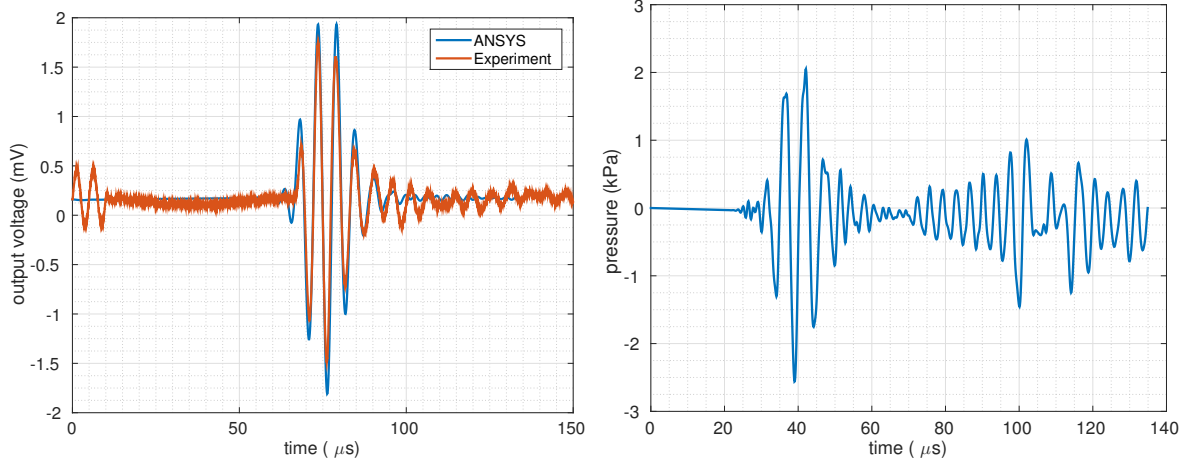


Figure 4.6: Comparison of experimental and analytical unamplified output signal (**left**), corresponding acoustic pressure (**right**). Reprinted from [73].

In response to an input pressure of 4 kPa_{pp} , the RX-CMUT (biased at 136 V) generates an output voltage of 3.30 mV_{pp} without any amplification. The produced voltage corresponds to a sensitivity of -241.7 dB (re $1 \text{ V}/1 \mu\text{Pa}$). The observed sensitivity is comparable to some commercially available piezoelectric based hydrophones and other adhesive-based wafer-bonded CMUT reported in the literature [41, 37]. The previously reported adhesive bonded CMUT has a transimpedance amplified sensitivity of -232.5 dB (re $1 \text{ V}/1 \mu\text{Pa}$) when operated at 3 MHz , whereas, the commercial hydrophone "BII-7181 Benthowave Instrument Inc." (Collingwood, Ontario, Canada) has a sensitivity of -240 dB (re $1 \text{ V}/1 \mu\text{Pa}$) without pre-amplification.

The applied biased voltage i.e 136 V DC is around 30% of the collapse voltage of the fabricated device, that is found to be around 450 V using the FEA analytical model. To incorporate the effect of the bias voltage on the sensitivity of the CMUT, the sensitivities has been calculated for higher bias voltages using the same analytical model. The output voltages against different bias voltages and their corresponding calculated sensitivities are illustrated in Figure 4.7. Comparative table for the sensitivity vs. bias voltage is demonstrated in Table 4.1.

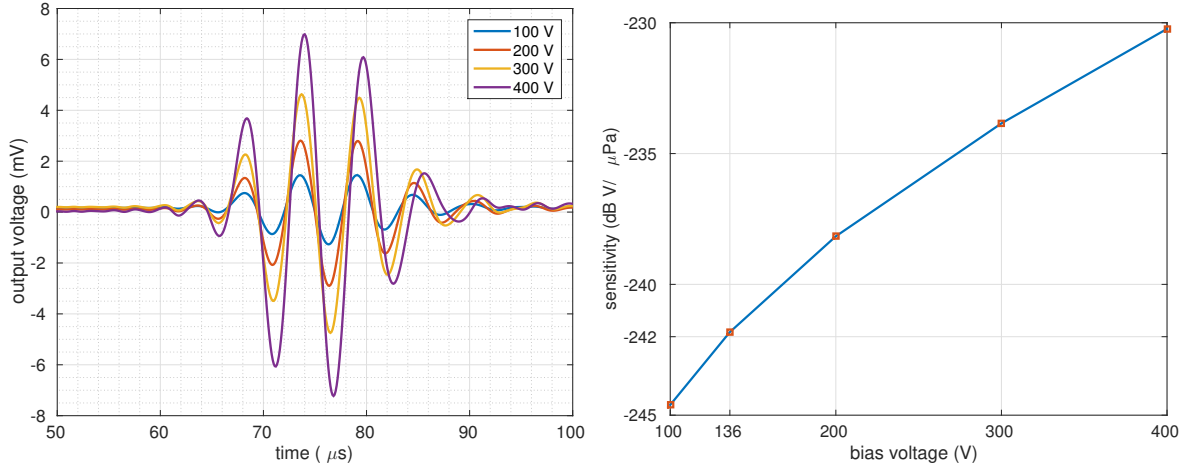


Figure 4.7: Simulated RX-CMUT output with varying bias voltage (**left**); associated sensitivity (**right**). Reprinted from [73].

Table 4.1: DC Bias Vs Output Sensitivity Comparison

DC Bias (V)	136	200	300	365	400
Sensitivity (dB re 1 V/1 μPa)	-241.7	-238	-234	-231.5	-230.1

As can be observed in the figure the sensitivity of the CMUT increases with increasing the bias voltage. Consequently, by applying a bias voltage of 364 V, which is 80% of the collapse voltage (455 V), sensitivity can be increased up to -231.5 dB (re 1 V/1 μPa).

In Figure 4.7 a drop in the resonance frequency of the CMUT is realized against an increase in the DC bias level. The drop in the resonance frequency with increase in the bias voltage is due to spring softening effect, a function of the applied DC bias. The applied DC voltage brings the membrane closer to the substrate, which results an increase in the electrical field. Hence, the membrane displaces more under an applied AC voltage as if the spring constant of the membrane has decreased. The spring-mass behaviour of the CMUT devices is briefly discussed by Brenner et al. in [52].

Chapter 5

Conclusion and Future Work

5.1 Conclusion

This thesis has focused on the development of an adhesive-based wafer-bonded CMUT fabrication process. PMMA is chosen to be the intermediate bonding layer in-between the bonded wafers. The use of expensive SOI wafers and complicated bonding equipment has been avoided to fabricate a low cost and simple CMUT device. A lab-built thermocompression bonding equipment is used in the fabrication process. Low cost, thermally oxidised silicon dioxide wafers have successfully been bonded to fabricate the CMUTs. The developed CMUTs have been designed for low frequency underwater applications and the entire thickness of the wafer have been utilized as the membrane. Other design parameters have subsequently been calculated analytically. The fabricated CMUTs have been experimentally characterized using static and dynamic methods. The static characterization has been carried out with the profilometer and the impedance analyzer. The impedance analyzer characterization shows that the fabricated CMUT is a power efficient device and the efficiency could be improved further with the application of the bias voltage. The dynamic characterization for measuring the bandwidth and the sensitivity has been carried out by performing a pitch-catch experiment. The sensitivity is found by matching the results of the experimental electrical measurements to the FEA model of the experimental setup. The transient analysis has been performed to calculate the sensitivity, whereas the bandwidth has been calculated

using the steady-state analysis. Conclusively, the obtained results are found to be comparable with the other adhesive-based wafer-bonded CMUTs reported in the literature and the commercially available piezoelectric devices.

In a nut shell, the process of characterization has provided an insight into an appropriate method of designing, fabricating and testing of the CMUTs.

5.2 Discussion and Future Work

The presented CMUT is specifically designed for low frequency underwater applications. This is an unconventional CMUT which uses the entire thickness of the wafer as the membrane. However, higher frequencies can also be achieved with PMMA based wafer bonding by reducing the membrane thickness, as the collapse voltage will drastically increase at the same membrane thickness if the radius is reduced for achieving higher operational frequencies. Membrane thickness can be reduced either by using a thin wafer or adopting the technique presented by [37, 38] with the cost of additional silicon etching and electrode deposition steps.

The fabricated CMUT element consist of 4×4 CMUT cells, the membrane supporting SiO_2 layer occupy 66 % of the the total CMUT element's area. The total insulating layer area must be optimized for better yield.

Another issue associated with the PMMA based bonding techniques is its inability to resist high temperatures and chemicals attack (acetone etc.), which adds a degree of care to the fabrication process.

For future development and fabrication of the CMUTs, three possible fabrication techniques are proposed.

5.2.1 Patterning Cavities in the Adhesive PMMA Layer

In the presented CMUT silicon dioxide SiO_2 has been used as an insulating and cavities patterning layer. To reduce the thickness of the insulation layer between the top and bottom electrodes, the PMMA adhesive bonding layer itself can be used to accommodate the cavity patterning as well as provide the electrical insulation between

the two electrodes. The cavities can be formed in one of the wafers using Electron Beam Lithography (EBL), while the second wafer can be coated with a thin PMMA layer to provide the insulation.

5.2.2 Membrane Silicon Layer Etching

The presented CMUT uses the entire thickness of the wafer as the membrane on purpose but the thick membrane results in a high collapse voltage. The collapse voltage drastically increase when the radius is reduced to achieve higher frequency keeping the membrane thickness constant. Therefore, for higher frequency of operation, the membrane thickness needs to be reduced to an optimal value to achieve a reasonable collapse voltage. In this regard, the silicon layer of the wafer can be etched with wet etching technique using silicon etchants such as, potassium hydroxide (KOH), leaving behind the oxide or nitride layer as the device layer. In the wet etch process the oxide/nitride layer will act as an etch stop layer as well. Since the heavily doped silicon wafer was used as one of the electrode, so a metal electrode layer would be deposited to form the top electrode.

5.2.3 Explore new Adhesive Materials

The major concern with PMMA as an adhesive material is its inability to resist chemical attacks are higher temperatures. In order to achieve better stability, adhesive materials with better chemical resistivity and temperature stability can be explored and investigated.

Appendix A

Finite Element Analysis

The pitch-catch experiment was modeled in ANSYS Multiphysics (ANSYS, Inc., Canonsburg, PA, USA) using the mesh structure depicted in Figure A.1. Only a quarter of a single transducer with symmetric boundary conditions were used in the model to reduce mesh size and simulation time. A column of oil was placed between two Si layers that acted as the plates of the transmitting and receiving transducers. FLUID30 and SOLID45 elements were used for modeling the oil and silicon layers, respectively.

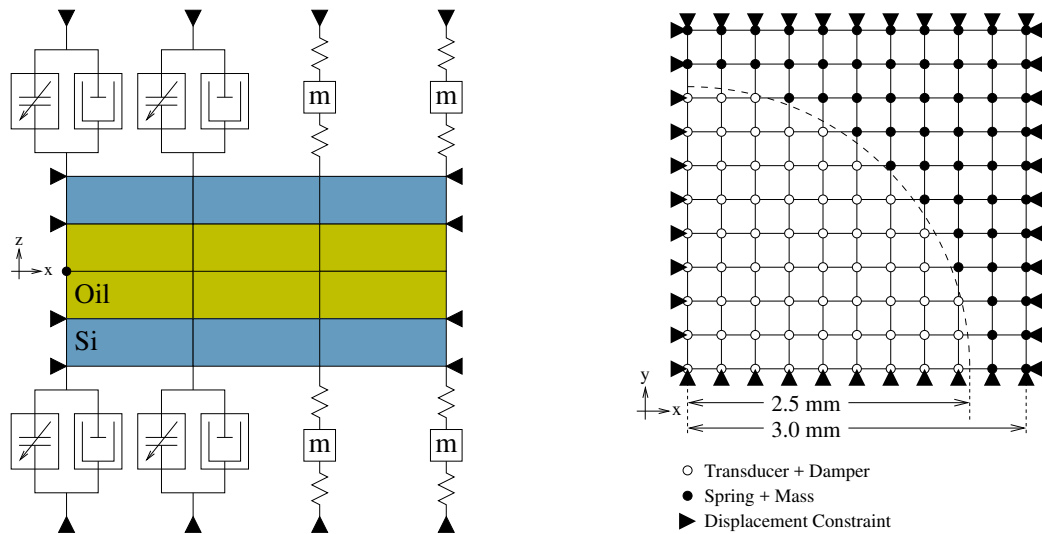


Figure A.1: Side view (with reduced element count) and top view of FEA model. Reprinted from [73].

The active area of the transducer is defined by placing TRANS126 Electromechan-

ical Transducer elements to nodes that are within a circle defining the radius of the transducer, while the remaining nodes are brought to contact with the bonding PMMA layer. Owing to the extremely unmatched relative thickness of the plate and PMMA layer (while the Si layer was 525 μm , the PMMA layer was only 200 nm thick) which would make meshing impractical, the PMMA layer was modeled using a pair of springs with a central mass. The transmitter was driven from the electrical port by 136 V DC bias and a two-cycle RF-burst of amplitude $10 V_{\text{pp}}$ at 200 kHz. The squeeze-film damping effect was modeled using COMBIN14 elements, whose damping coefficients were empirically found based on experiment data. The model had 10×10 elements in the xy plane, while the fluid column of 10 cm height was meshed using 10 elements per acoustic wavelength at 200 kHz, totaling 14,428 elements, and 17,058 nodes. Table A.1 lists the simulation parameters.

Table A.1: Simulation parameters.

Parameter	Value	Units
Young's modulus of Si	130	GPa
Poisson's ratio of Si	0.27	–
Mass density of Si	2280	kg/m^3
Speed of sound in oil	1500	m/s
Mass density of oil	1000	kg/m^3
Young's modulus of PMMA	3	GPa
Mass density of PMMA	1185	kg/m^3
Damping coefficient	0.06	$\text{N} \cdot \text{s}/\text{m}$

Appendix B

Squeeze Film Damping

The bonding equipment used in the manufacturing of the devices was operated at low-vacuum levels, due to which the squeeze-film damping effect was observed. Linearized compressible Reynolds equation could be used to study the conduct of trapped air between two parallel vibrating plates [77]. In a solution for parallel-moving vented circular plates, Blech [78] showed that dimensionless viscous and elastic damping behavior is dependent on squeeze number (σ), given in Equation (B.1).

$$\sigma = 12\mu_{\text{eff}} \frac{\omega}{p_a} \left(\frac{a}{g_h} \right)^2 \quad (\text{B.1})$$

where p_a the ambient pressure, a/g_h is the radius to cavity height ratio, ω is the angular oscillation frequency and μ_{eff} is the rarefaction effect and expressed as follows.

$$\mu_{\text{eff}} = \frac{\mu}{1 + 9.638 K_n^{1.159}} \quad (\text{B.2})$$

where μ is the dynamic viscosity of air, and $K_n = \lambda/g_h$ is the Knudsen number. The mean free path of air (λ) depends on air-pressure level (P) and air density (ρ) within the cavity, and is given by the following expression [79]:

$$\lambda = \frac{\mu}{u} \sqrt{\frac{\pi}{8\rho P}} \quad (\text{B.3})$$

where u is a numerical factor equal to 0.4987445.

The parameters used in the above expressions for squeeze-number calculation and their corresponding values are summarized in Table B.1.

Table B.1: Squeeze-number computation parameters.

Parameter	Value	Units
Dynamic viscosity of air μ	1.825×10^{-5}	Kg/m·s
Angular frequency ω	1.26×10^6	rad/s
Membrane radius a	2.5	mm
Cavity height g_0	800	nm
Ambient pressure P_a	101,325	Pa
Cavity pressure P	from Table B.2	Pa
Density of air ρ	from Table B.2	kg/m ³
Mean free path of air λ	from Table B.2	nm

The squeeze number at different cavity pressure levels is calculated by inserting Expressions (B.2) and (B.3) into Equation (B.1), as presented in Table B.2.

Table B.2: Squeeze number at different pressure levels.

Pressure (Pa)	Density (kg/m ³)	Mean Free Path, λ (nm)	Squeeze Number
100,000	1.16864	67.99	17,300
10,000	0.116864	679.9	2990
1000	0.0116864	6799	231
500	0.00584	13,599	104
300	0.00351	22,665	58

Since the CMUT acts like a flexible plate instead of a rigid piston, the nonuniform deflection of the membrane results in nonuniform distribution of pressure within the cavity. Due to the pressure difference, air flows from higher-pressure regions to lower-pressure regions in the sealed cavity, which consequently results in viscous loss [80, 81]. Galisultanov et al. investigated the damping effect in CMUTs and revealed that, for a squeeze number higher than 50, CMUTs possess a damping effect as, at a high squeeze number, the viscous damping force is similar for both sealed and open cavities [80, 81].

The data in Table B.2 show that the proposed CMUT carries a damping effect for the cavity pressure of as low as 300 Pa as per the findings of References [80, 81].

Bibliography

- [1] M. I. Haller and B. T. Khuri-Yakub, “A surface micromachined electrostatic ultrasonic air transducer,” *IEEE transactions on ultrasonics, ferroelectrics, and frequency control*, vol. 43, no. 1, pp. 1–6, 1996.
- [2] M. I. Haller and B. T. Khuri-Yakub, “Electrostatic ultrasonic transducer,” Apr. 8 1997. US Patent 5,619,476.
- [3] L. Jia, C. He, C. Xue, and W. Zhang, “The device characteristics and fabrication method of 72-element cmut array for long-range underwater imaging applications,” *Microsystem Technologies*, pp. 1–8, 2018.
- [4] S. Vaithilingam, T.-J. Ma, Y. Furukawa, I. O. Wygant, X. Zhuang, A. De La Zerda, O. Oralkan, A. Kamaya, R. B. Jeffrey, B. T. Khuri-yakub, *et al.*, “Three-dimensional photoacoustic imaging using a two-dimensional cmut array,” *IEEE transactions on ultrasonics, ferroelectrics, and frequency control*, vol. 56, no. 11, pp. 2411–2419, 2009.
- [5] R. K. Chee, P. Zhang, M. Maadi, and R. J. Zemp, “Multifrequency interlaced cmuts for photoacoustic imaging,” *IEEE transactions on ultrasonics, ferroelectrics, and frequency control*, vol. 64, no. 2, pp. 391–401, 2016.
- [6] R. Zhang, W. Zhang, C. He, J. Song, L. Mu, J. Cui, Y. Zhang, and C. Xue, “Design of capacitive micromachined ultrasonic transducer (cmut) linear array for underwater imaging,” *Sensor Review*, vol. 36, no. 1, pp. 77–85, 2016.
- [7] A. Logan and J. T. Yeow, “Fabricating capacitive micromachined ultrasonic transducers with a novel silicon-nitride-based wafer bonding process,” *IEEE transactions*

- on ultrasonics, ferroelectrics, and frequency control*, vol. 56, no. 5, pp. 1074–1084, 2009.
- [8] A. Caronti, G. Caliano, R. Carotenuto, A. Savoia, M. Pappalardo, E. Cianci, and V. Foglietti, “Capacitive micromachined ultrasonic transducer (cmut) arrays for medical imaging,” *Microelectronics Journal*, vol. 37, no. 8, pp. 770–777, 2006.
- [9] A. Erguri, Y. Huang, X. Zhuang, O. Oralkan, G. G. Yarahoglu, and B. T. Khuri-Yakub, “Capacitive micromachined ultrasonic transducers: Fabrication technology,” *IEEE transactions on ultrasonics, ferroelectrics, and frequency control*, vol. 52, no. 12, pp. 2242–2258, 2005.
- [10] J. J.-Q. Lu, P. Ramm, and M. M. Taklo, *Handbook of Wafer Bonding*. Wiley Online Library, 2012.
- [11] Y. Tsuji, M. Kupnik, and B. T. Khuri-Yakub, “Low temperature process for cmut fabrication with wafer bonding technique,” in *2010 IEEE International Ultrasonics Symposium*, pp. 551–554, IEEE, 2010.
- [12] S. Bengtsson and P. Amirfeiz, “Room temperature wafer bonding of silicon, oxidized silicon, and crystalline quartz,” *Journal of Electronic Materials*, vol. 29, no. 7, pp. 909–915, 2000.
- [13] J. Zahorian, R. Guldiken, G. Gurun, M. S. Qureshi, M. Balantekin, P. Hasler, and F. L. Degertekin, “Single chip cmut arrays with integrated cmos electronics: Fabrication process development and experimental results,” in *2008 IEEE ultrasonics symposium*, pp. 386–389, IEEE, 2008.
- [14] G. Gurun, C. Tekes, J. Zahorian, T. Xu, S. Satir, M. Karaman, J. Hasler, and F. L. Degertekin, “Single-chip cmut-on-cmos front-end system for real-time volumetric ivus and ice imaging,” *IEEE transactions on ultrasonics, ferroelectrics, and frequency control*, vol. 61, no. 2, pp. 239–250, 2014.
- [15] J. Zahorian, M. Hochman, T. Xu, S. Satir, G. Gurun, M. Karaman, and F. L. Degertekin, “Monolithic cmut-on-cmos integration for intravascular ultrasound ap-

- plications,” *IEEE transactions on ultrasonics, ferroelectrics, and frequency control*, vol. 58, no. 12, pp. 2659–2667, 2011.
- [16] G. Gurun, P. Hasler, and F. L. Degertekin, “Front-end receiver electronics for high-frequency monolithic cmut-on-cmos imaging arrays,” *IEEE transactions on ultrasonics, ferroelectrics, and frequency control*, vol. 58, no. 8, pp. 1658–1668, 2011.
- [17] R. Goyal and D. M. Yadav, “Design and simulation of a mems-based capacitive micro-machined ultrasonic transducer for viscosity sensing applications,”
- [18] S. Park, I. Yoon, S. Lee, H. Kim, J.-W. Seo, Y. Chung, A. Unger, M. Kupnik, and H. J. Lee, “Cmut-based resonant gas sensor array for voc detection with low operating voltage,” *Sensors and Actuators B: Chemical*, vol. 273, pp. 1556–1563, 2018.
- [19] S. Fanget, S. Hentz, P. Puget, J. Arcamone, M. Matheron, E. Colinet, P. Andreucci, L. Duraffourg, E. Myers, and M. Roukes, “Gas sensors based on gravimetric detection—a review,” *Sensors and Actuators B: Chemical*, vol. 160, no. 1, pp. 804–821, 2011.
- [20] O. Farhanieh, A. Sahafi, R. B. Roy, A. S. Ergun, and A. Bozkurt, “Integrated hifu drive system on a chip for cmut-based catheter ablation system,” *IEEE transactions on biomedical circuits and systems*, vol. 11, no. 3, pp. 534–546, 2017.
- [21] S. H. Wong, R. D. Watkins, M. Kupnik, K. B. Pauly, and B. T. Khuri-Yakub, “Feasibility of mr-temperature mapping of ultrasonic heating from a cmut,” *IEEE transactions on ultrasonics, ferroelectrics, and frequency control*, vol. 55, no. 4, pp. 811–818, 2008.
- [22] D. Gross, M. Legros, P. Vince, and D. Certon, “Evaluation of an ultrasound-guided focused ultrasound cmut probe for targeted therapy applications,” *Open Journal of Applied Sciences*, vol. 8, no. 01, p. 25, 2018.

- [23] D. Hah, C. H. Je, and S.-Q. Lee, "Design of capacitive micromachined ultrasonic transducers (cmuts) on a flexible substrate for intravascular ultrasonography (ivus) applications," in *2017 Symposium on Design, Test, Integration and Packaging of MEMS/MOEMS (DTIP)*, pp. 1–5, IEEE, 2017.
- [24] M. Wang and J. Chen, "Volumetric flow measurement using an implantable cmut array," *IEEE transactions on biomedical circuits and systems*, vol. 5, no. 3, pp. 214–222, 2011.
- [25] M. Wang, J. Chen, X. Cheng, T. Zhang, and X. Liu, "A bi-directional real-time blood flowmeter using an implantable cmut array," in *2008 IEEE Ultrasonics Symposium*, pp. 1–4, IEEE, 2008.
- [26] R. Przybyla, A. Flynn, V. Jain, S. Shelton, A. Guedes, I. Izyumin, D. Horsley, and B. Boser, "A micromechanical ultrasonic distance sensor with > 1 meter range," in *2011 16th International Solid-State Sensors, Actuators and Microsystems Conference*, pp. 2070–2073, IEEE, 2011.
- [27] S. Berg and A. Ronnekleiv, "5f-5 reducing fluid coupled crosstalk between membranes in cmut arrays by introducing a lossy top layer," in *2006 IEEE Ultrasonics Symposium*, pp. 594–597, IEEE, 2006.
- [28] S. Zhou and J. A. Hossack, "Reducing inter-element acoustic crosstalk in capacitive micromachined ultrasound transducers," *IEEE transactions on ultrasonics, ferroelectrics, and frequency control*, vol. 54, no. 6, pp. 1217–1228, 2007.
- [29] S. Na, A. I. Chen, L. L. Wong, Z. Li, M. Macecek, and J. T. Yeow, "Capacitive micromachined ultrasonic transducers based on annular cell geometry for air-coupled applications," *Ultrasonics*, vol. 71, pp. 152–160, 2016.
- [30] I. Albert, H. Chen, L. L. Wong, S. Na, Z. Li, M. Macecek, and J. T. Yeow, "Fabrication of a curved row-column addressed capacitive micromachined ultrasonic transducer array," *Journal of Microelectromechanical Systems*, vol. 25, no. 4, pp. 675–682, 2016.

- [31] A. Caronti, A. Coppa, A. Savoia, C. Longo, P. Gatta, B. Mauti, A. Corbo, B. Calabrese, G. Bollino, A. Paz, *et al.*, “Curvilinear capacitive micromachined ultrasonic transducer (cmut) array fabricated using a reverse process,” in *2008 IEEE Ultrasonics Symposium*, pp. 2092–2095, IEEE, 2008.
- [32] G. Caliano, A. Caronti, A. Savoia, C. Longo, M. Pappalardo, E. Cianci, and V. Foglietti, “Capacitive micromachined ultrasonic transducer (cmut) made by a novel" reverse fabrication process",” in *IEEE Ultrasonics Symposium, 2005.*, vol. 1, pp. 479–482, IEEE, 2005.
- [33] A. Bozkurt, I. Ladabaum, A. Atalar, and B. T. Khuri-Yakub, “Theory and analysis of electrode size optimization for capacitive microfabricated ultrasonic transducers,” *ieee transactions on ultrasonics, ferroelectrics, and frequency control*, vol. 46, no. 6, pp. 1364–1374, 1999.
- [34] K. Park, H. Lee, M. Kupnik, O. Oralkan, and B. Khuri-Yakub, “Fabricating capacitive micromachined ultrasonic transducers with direct wafer-bonding and locos technology,” in *2008 IEEE 21st International Conference on Micro Electro Mechanical Systems*, pp. 339–342, IEEE, 2008.
- [35] Y. Huang, A. S. Ergun, E. Haeggstrom, M. H. Badi, and B. T. Khuri-Yakub, “Fabricating capacitive micromachined ultrasonic transducers with wafer-bonding technology,” *Journal of microelectromechanical systems*, vol. 12, no. 2, pp. 128–137, 2003.
- [36] M. Bellaredj, G. Bourbon, V. Walter, P. Le Moal, and M. Berthillier, “Anodic bonding using soi wafer for fabrication of capacitive micromachined ultrasonic transducers,” *Journal of Micromechanics and Microengineering*, vol. 24, no. 2, p. 025009, 2014.
- [37] Z. Li, L. L. Wong, A. I. Chen, S. Na, J. Sun, and J. T. Yeow, “Fabrication of capacitive micromachined ultrasonic transducers based on adhesive wafer bonding technique,” *Journal of Micromechanics and Microengineering*, vol. 26, no. 11, p. 115019, 2016.

- [38] A. S. Havreland, M. L. Ommen, C. Silvestre, M. Engholm, E. V. Thomsen, *et al.*, “Bcb polymer based row-column addressed cmut,” in *2017 IEEE International Ultrasonics Symposium (IUS)*, pp. 1–4, IEEE, 2017.
- [39] Z. Li, S. Na, A. I. Chen, L. L. Wong, Z. Sun, P. Liu, and J. T. Yeow, “Optimization on benzocyclobutene-based cmut fabrication with an inverse structure,” *Sensors and Actuators A: Physical*, vol. 281, pp. 1–8, 2018.
- [40] J. Joseph, S. G. Singh, and S. R. K. Vanjari, “Fabrication and characterization of su-8-based capacitive micromachined ultrasonic transducer for airborne applications,” *Journal of Micro/Nanolithography, MEMS, and MOEMS*, vol. 17, no. 1, p. 015003, 2018.
- [41] BENTHOWAVE INSTRUMENT INC., “BII-7180 Series Miniature Probe Hydrophone,” <https://www.benthowave.com/products/BII-7180Hydrophone.html>, accessed on 05.04.2019.
- [42] H. Soh, I. Ladabaum, A. Atalar, C. Quate, and B. Khuri-Yakub, “Silicon micromachined ultrasonic immersion transducers,” *Applied Physics Letters*, vol. 69, no. 24, pp. 3674–3676, 1996.
- [43] B. T. Khuri-Yakub, C.-H. Cheng, F.-L. Degertekin, S. Ergun, S. Hansen, X.-C. Jin, and O. Oralkan, “Silicon micromachined ultrasonic transducers,” *Japanese Journal of Applied Physics*, vol. 39, no. 5S, p. 2883, 2000.
- [44] E. Cianci, L. Visigalli, V. Foglietti, G. Caliano, and M. Pappalardo, “Improvements towards a reliable fabrication process for cmut,” *Microelectronic Engineering*, vol. 67, pp. 602–608, 2003.
- [45] S. Calmes, C. Cheng, F. Degertekin, X. Jin, S. Ergun, and B. Khuri-Yakub, “Highly integrated 2-d capacitive micromachined ultrasonic transducers,” in *1999 IEEE Ultrasonics Symposium. Proceedings. International Symposium (Cat. No. 99CH37027)*, vol. 2, pp. 1163–1166, IEEE, 1999.

- [46] A. Buhrdorf, L. Tebje, O. Ahrens, O. Glitza, and J. Binder, “Capacitive micromachined ultrasonic transducer (cmut) array for the frequency range below 500 khz,” in *2000 IEEE Ultrasonics Symposium. Proceedings. An International Symposium (Cat. No. 00CH37121)*, vol. 1, pp. 915–918, IEEE, 2000.
- [47] M. Pappalardo, G. Caliano, A. Caronti, F. D’alessio, C. Cucco, E. Cianci, and V. Foglietti, “Capacitive ultrasonic transducers with a new vibrating structure,” in *IEEE Symposium on Ultrasonics, 2003*, vol. 2, pp. 1955–1959, IEEE, 2003.
- [48] R. B. Roy, O. Farhanieh, A. S. Ergün, and A. Bozkurt, “Fabrication of high-efficiency cmuts with reduced parasitics using embedded metallic layers,” *IEEE Sensors Journal*, vol. 17, no. 13, pp. 4013–4020, 2017.
- [49] Y. Huang, A. Ergun, E. Haeggstrom, and B. Khuri-Yakub, “Fabrication of capacitive micromachined ultrasonic transducers (cmuts) using wafer bonding technology for low frequency (10 khz-150 khz) sonar applications,” in *OCEANS’02 MTS/IEEE*, vol. 4, pp. 2322–2327, IEEE, 2002.
- [50] Z. Li, L. L. Wong, A. I. Chen, S. Na, J. Sun, and J. T. Yeow, “Fabrication of capacitive micromachined ultrasonic transducers based on adhesive wafer bonding technique,” *Journal of Micromechanics and Microengineering*, vol. 26, no. 11, p. 115019, 2016.
- [51] Y. Huang, A. S. Ergun, E. Haeggstrom, M. H. Badi, and B. T. Khuri-Yakub, “Fabricating capacitive micromachined ultrasonic transducers with wafer-bonding technology,” *Journal of microelectromechanical systems*, vol. 12, no. 2, pp. 128–137, 2003.
- [52] K. Brenner, A. S. Ergun, K. Firouzi, M. F. Rasmussen, Q. Stedman, and B. P. Khuri-Yakub, “Advances in capacitive micromachined ultrasonic transducers,” *Micromachines*, vol. 10, no. 2, p. 152, 2019.
- [53] M. Taklo, P. Storås, K. Schjølberg-Henriksen, H. Hasting, and H. Jakobsen, “Strong, high-yield and low-temperature thermocompression silicon wafer-level

- bonding with gold,” *Journal of Micromechanics and Microengineering*, vol. 14, no. 7, p. 884, 2004.
- [54] Z. Li, L. Zhao, Z. Jiang, P. Li, Y. Hu, and Y. Zhao, “Fabrication of cmuts with a low temperature wafer bonding technology,” in *2015 IEEE SENSORS*, pp. 1–4, IEEE, 2015.
- [55] G. Wallis and D. I. Pomerantz, “Field assisted glass-metal sealing,” *Journal of applied physics*, vol. 40, no. 10, pp. 3946–3949, 1969.
- [56] A. Gerlach, D. Maas, D. Seidel, H. Bartuch, S. Schundau, and K. Kaschlik, “Low-temperature anodic bonding of silicon to silicon wafers by means of intermediate glass layers,” *Microsystem technologies*, vol. 5, no. 3, pp. 144–149, 1999.
- [57] F. Y. Yamaner, S. Olcum, H. K. Oguz, A. Bozkurt, H. Koymen, and A. Atalar, “High-power cmuts: design and experimental verification,” *IEEE transactions on ultrasonics, ferroelectrics, and frequency control*, vol. 59, no. 6, pp. 1276–1284, 2012.
- [58] F. Y. Yamaner, X. Zhang, and Ö. Oralkan, “A three-mask process for fabricating vacuum-sealed capacitive micromachined ultrasonic transducers using anodic bonding,” *IEEE transactions on ultrasonics, ferroelectrics, and frequency control*, vol. 62, no. 5, pp. 972–982, 2015.
- [59] F. Niklaus, G. Stemme, J.-Q. Lu, and R. Gutmann, “Adhesive wafer bonding,” *Journal of applied physics*, vol. 99, no. 3, p. 2, 2006.
- [60] X. Zhang, O. Adelegan, F. Y. Yamaner, and Ö. Oralkan, “An optically transparent capacitive micromachined ultrasonic transducer (cmut) fabricated using su-8 or bcb adhesive wafer bonding,” in *2017 IEEE International Ultrasonics Symposium (IUS)*, pp. 1–4, IEEE, 2017.
- [61] A. Bakhtazad, R. Manwar, and S. Chowdhury, “Fabrication and characterization of sealed cavities realized by adhesive wafer bonding with dry etched cyclotene™,” *Microsystem Technologies*, vol. 21, no. 11, pp. 2435–2442, 2015.

- [62] F. Blanco, M. Agirregabiria, J. Garcia, J. Berganzo, M. Tijero, M. Arroyo, J. Ruano, I. Aramburu, and K. Mayora, “Novel three-dimensional embedded su-8 microchannels fabricated using a low temperature full wafer adhesive bonding,” *Journal of Micromechanics and Microengineering*, vol. 14, no. 7, p. 1047, 2004.
- [63] W. P. Eaton, S. H. Risbud, and R. L. Smith, “Silicon wafer-to-wafer bonding at $t < 200^\circ \text{C}$ with polymethylmethacrylate,” *Applied physics letters*, vol. 65, no. 4, pp. 439–441, 1994.
- [64] W. W. Flack, D. S. Soong, A. T. Bell, and D. W. Hess, “A mathematical model for spin coating of polymer resists,” *Journal of Applied Physics*, vol. 56, no. 4, pp. 1199–1206, 1984.
- [65] D. B. Hall, P. Underhill, and J. M. Torkelson, “Spin coating of thin and ultrathin polymer films,” *Polymer Engineering & Science*, vol. 38, no. 12, pp. 2039–2045, 1998.
- [66] Y. Ohama, T. Kobayashi, K. Takeuchi, and K. Nawata, “Chemical resistance of polymethyl methacrylate concrete,” *International Journal of Cement Composites and Lightweight Concrete*, vol. 8, no. 2, pp. 87–91, 1986.
- [67] K. S. Khare, F. Khabaz, and R. Khare, “Effect of carbon nanotube functionalization on mechanical and thermal properties of cross-linked epoxy-carbon nanotube nanocomposites: role of strengthening the interfacial interactions,” *ACS applied materials & interfaces*, vol. 6, no. 9, pp. 6098–6110, 2014.
- [68] E. M. Jackson, P. E. Laibinis, W. E. Collins, A. Ueda, C. D. Wingard, and B. Penn, “Development and thermal properties of carbon nanotube-polymer composites,” *Composites Part B: Engineering*, vol. 89, pp. 362–373, 2016.
- [69] I. O. Wygant, M. Kupnik, and B. T. Khuri-Yakub, “Analytically calculating membrane displacement and the equivalent circuit model of a circular cmut cell,” in *2008 IEEE Ultrasonics Symposium*, pp. 2111–2114, IEEE, 2008.

- [70] J. L. Sutton, "Underwater acoustic imaging," *Proceedings of the IEEE*, vol. 67, no. 4, pp. 554–566, 1979.
- [71] A. Bozkurt and G. G. Yaralioglu, "Receive-noise analysis of capacitive micromachined ultrasonic transducers," *IEEE Transactions on Ultrasonics, Ferroelectrics, and Frequency Control*, vol. 63, pp. 1980–1987, Nov 2016.
- [72] X. Zhuang, *Capacitive micromachined ultrasonic transducers with through-wafer interconnects*. Stanford University, 2008.
- [73] M. Ahmad, A. Bozkurt, and O. Farhanieh, "Pmma-based wafer-bonded capacitive micromachined ultrasonic transducer for underwater applications," *Micromachines*, vol. 10, no. 5, p. 319, 2019.
- [74] D. Gross, A. Boulmé, N. Sénégon, C. Bawiec, W. A. N'Djin, and D. Certon, "Analysis of cmut power efficiency for optimized therapeutic operation," in *2017 IEEE International Ultrasonics Symposium (IUS)*, pp. 1–4, IEEE, 2017.
- [75] J. N. Coupland and D. J. McClements, "Physical properties of liquid edible oils," *Journal of the American Oil Chemists' Society*, vol. 74, no. 12, pp. 1559–1564, 1997.
- [76] R. Chanamai and D. J. McClements, "Ultrasonic attenuation of edible oils," *Journal of the American Oil Chemists' Society*, vol. 75, no. 10, pp. 1447–1448, 1998.
- [77] M. Bao and H. Yang, "Squeeze film air damping in mems," *Sensors and Actuators A: Physical*, vol. 136, no. 1, pp. 3–27, 2007.
- [78] J. J. Blech, "On isothermal squeeze films," *Journal of lubrication technology*, vol. 105, no. 4, pp. 615–620, 1983.
- [79] S. Jennings, "The mean free path in air," *Journal of Aerosol Science*, vol. 19, no. 2, pp. 159–166, 1988.

- [80] A. Galisultanov, P. Le Moal, V. Walter, and G. Bourbon, “Dynamic characteristics of circular cmuts with air-filled cavities,” in *2016 IEEE International Ultrasonics Symposium (IUS)*, pp. 1–4, IEEE, 2016.
- [81] A. Galisultanov, P. Le Moal, G. Bourbon, and V. Walter, “Squeeze film damping and stiffening in circular cmut with air-filled cavity: Influence of the lateral venting boundary conditions and the bias voltage,” *Sensors and Actuators A: Physical*, vol. 266, pp. 15–23, 2017.